SAND REPORT

SAND2002-8609
Unlimited Release
Printed January 2003

Evaluation of NASA Lean Premixed Hydrogen Burner

R.W. Schefer, T. D. Smith, C. J. Marek

Prepared by
Sandia National Laboratories
Albuquerque, New Mexico 87185 and Livermore, California 94550

Sandia is a multiprogram laboratory operated by Sandia Corporation, a Lockheed Martin Company, for the United States Department of Energy's National Nuclear Security Administration under Contract DE-AC04-94-AL85000.

Sandia National Laboratories

Issued by Sandia National Laboratories, operated for the United States Department of Energy by Sandia Corporation.

Available to DOE and DOE contractors from
U.S. Department of Energy
Office of Scientific and Technical Information
P.O. Box 62
Oak Ridge, TN 37831

Telephone: (865)576-8401
Facsimile: (865)576-5728
E-Mail: reports@adonis.osti.gov
Online ordering: http://www.doe.gov/bridge

Available to the public from
U.S. Department of Commerce
National Technical Information Service
5285 Port Royal Rd
Springfield, VA 22161

Telephone: (800)553-6847
Facsimile: (703)605-6900
E-Mail: orders@ntis.fedworld.gov
Online order: http://www.ntis.gov/help/ordermethods.asp?loc=7-4-0#online

SAND2002-8609

SAND2002-8609
Unlimited Release
Printed January 2003

Evaluation of NASA Lean Premixed Hydrogen Burner

R.W. Schefer
Combustion Research Facility
Sandia National Laboratories
Livermore, CA 94551-0969

T. D. Smith and C. J. Marek
NASA Glenn Research Center
Cleveland, OH 44135

Abstract

The stability characteristics of a prototype premixed, hydrogen-fueled burner were studied. The potential application is the use of hydrogen as a fuel for aircraft gas turbine operation. The burner configuration consisted of nine 6.72 mm (0.265 in) diameter channels through which the reactants entered the burner. Hydrogen was injected radially inward through two 0.906-mm (0.0357 in) diameter holes located on opposite sides of each air channel. In this way the region over which hydrogen and air were premixed was minimized to prevent potential flashback problems. All tests were carried out at atmospheric pressure. Flame stability was studied over a range of fuel-lean operating conditions since lean combustion is currently recognized as an effective approach to NO_x emissions reduction. In addition to pure hydrogen and air, mixtures of hydrogen-blended methane and air were studied to evaluate the potential improvements in flame stability as hydrogen replaces methane as the primary fuel component.

Contents

Abstract 3
Contents 4
Introduction 5
Experimental System 7
  Burner Description and Flow Conditions 7
  OH Fluorescence Imaging 8
  Acetone Fluorescence Imaging 9
Experimental Results 10
  Unconfined Flame Configuration 10
  Confined Flame Configuration 13
  Mixing Behavior using Acetone PLIF Imaging 17
Summary 19
Possible Future Work 19
Acknowledgements 19
Bibliography 20
Appendix I 22
Appendix II 23
Distribution 49

Introduction

The development of advanced combustion capabilities for gaseous hydrogen and hydrogen-blended hydrocarbon fuels in gas turbine applications is an area of much current interest. Driving this interest are several current needs. One need is the cost-effective utilization of alternative fuels with a wide range of heating values. For example, low and medium heating value fuels containing significant hydrogen are often produced as a by-product in Coal-Gasification Combined Cycle and Fluidized Bed Combustion installations. These product gases could provide a significant source of cost-effective fuels for gas turbines. A second need is related to the recognition that ultra-lean premixed combustion is an effective approach to NO_x emissions reduction from gas turbine engines. Hydrogen blended with traditional hydrocarbon fuels significantly improves flame stability during lean combustion and allows stable combustion at the low temperatures needed to minimize NO_x production. A longer-term need is the desire to eliminate UHC and CO_2 emissions. The use of hydrogen and hydrogen-blended hydrocarbon fuels provides both a solution to the immediate need for NO_x reduction, and also provides a transition strategy to a carbon free energy system in the future.

Changes in fuel composition, particularly the addition of hydrogen to hydrocarbon fuels, affect both the chemical and physical processes occurring in flames. These changes affect flame stability, combustor acoustics, pollutant emissions, combustor efficiency and other important quantities. Few of these issues are clearly understood. Studies in the literature related to the use of hydrogen as both the primary fuel and a fuel additive have been directed toward the effects of small amounts of hydrogen addition on hydrocarbon flame stability and pollutant formation under fuel-lean conditions. For example, studies in spark ignition engines clearly show the benefits of hydrogen blended with natural gas on exhaust emissions (Larson and Wallace, 1997) and on extending the lean engine operating limits (Meyers and Kubesh, 1997; Bell and Gupta, 1997). Early results in large-scale gas turbine combustors also indicate advantages to hydrogen addition. Clayton (1976) carried out a study on the effect of hydrogen addition in aircraft gas turbines. Up to 15% hydrogen addition to JP-5 or JP-6 produced leaner blowout limits and corresponding reductions in NO_x (less than 10 ppm @ 15% O2) while maintaining acceptable CO and HC emissions levels. Anderson (1975) premixed hydrogen with propane (up to 5% of the total fuel flow) to show that H_2 addition extended the premixed lean flammability limits and improved combustion efficiency. These tests were carried out at reactant inlet temperatures up to 700K and pressures up to 5 atm. In a subsequent study (Anderson, 1976), experiments using premixed hydrogen and air demonstrated NO_x emission levels of 0.06 ppm and combustion efficiency of 98% at an equivalence ratio of 0.24. Tests conducted in a single combustor test stand at full pressure and temperature at the GE Corporate Research and Development Center demonstrated improved flame stability with hydrogen addition to natural gas fuel (Morris et al., 1998). Blends of up to 10% hydrogen by volume showed reduced CO emissions with increased hydrogen addition under lean conditions, and lower NO_x emissions for a given CO level.

At a more fundamental level, the results of stretched flame calculations at elevated pressure (30 atm) (Gauducheau et al., 1998) showed that the improved lean flame stability was attributed to hydrogen's higher flame speed and increased resistance to strain. It was further noted that flame radical concentrations (O, H and OH) increased significantly with hydrogen addition in strained flames. These observations are consistent with the speculations of Phillips and Roby (1999) who attributed the enhanced reaction rates with hydrogen to an increase in the radical pool.

The objective of the present work is to evaluate the stability characteristics of a prototype fuel-lean, premixed burner designed for use with hydrogen as a fuel. The long-term emphasis is on the use of pure hydrogen. However, results using mixtures of hydrogen blended with methane are also presented in an effort to extend previous literature studies that considered the addition of only small amounts (typically less than 20% by volume) of hydrogen to hydrocarbon flames.

In the remainder of the paper the experimental system and burner will be described. Results characterizing the combustion stability of the burner at atmospheric pressure will be presented with an emphasis on understanding flame stability under increasingly fuel-lean conditions. A major goal of the present work is to evaluate the performance of the burner design with regard to premixing of the fuel and air. It is hoped that these results will form the basis for burner design improvements.

Experimental System

Burner Description and Flow Conditions

A schematic of the burner apparatus is shown in Fig. 1. The burner, which is operated at atmospheric pressure, consists of nine 6.72-mm (0.265 in) diameter holes, or channels, in an injector base plate through which the reactants enter the burner combustion section. Pure air enters the channels through the back plane of the base plate, while hydrogen is injected radially inward through two 0.906-mm (0.0357 in) diameter holes located on opposite sides of each air channel. The holes in the sides of the air channels can be seen in the photograph of the injector base plate in Fig. 1b. The fuel enters the injector base plate through four 6.35-mm (0.25 in) stainless steel tubes that extend radially outward from the base plate, as seen in Fig. 1a. The fuel stream circulates through several passages in the base plate before being injected into the air stream. In this way, the base plate injector is cooled by the circulating fuel, which effectively preheats the fuel stream prior to mixing with the air. The inlet air is unheated at a temperature of 293 K prior to mixing with the fuel. The fuel injection holes are located 7.62 mm (0.3 in) upstream of the inlet to the burner combustion section. In this way, the region over which hydrogen and air are premixed is minimized to prevent potential flashback problems. A 1-m (39.4 in) straight length of 38-mm (1.5 in) diameter pipe upstream of the base plate provides a fully-turbulent air flow. Air is radially injected into the bottom the straight inlet pipe through four 6.35-mm (0.25 in) diameter tubes equally spaced around the inlet pipe circumference. At the maximum airflow rate of nearly 2100 slm (74.1 ft^3/m), this corresponds to a Mach number at each tube exit of 0.7. The confinement section of the combustor is provided with four flat quartz windows that provide optical access for visual observation and for the application of laser-diagnostics. The combustor confinement walls are uncooled. The exit flow of hot combustion gases expands into ambient room air at atmospheric pressure, which provides an acoustically soft exit boundary condition. Combustion air is provided by an air compressor and metered upstream of the burner using mass flow meters for flow rates up to 2000 slm (70.6 ft^3/m). The air is dried and filtered to remove particles by suitable in-line filters. The fuels, methane and hydrogen, are metered using mass flow meters. The mass flow meters are calibrated using laminar flow elements to an estimated accuracy of 2%. Typical inlet Reynolds numbers for the detailed results presented in the following section vary from 11,456 to nearly 36,000 (see Appendix).

OH Fluorescence Imaging

A schematic of the experimental setup for OH fluorescence imaging is shown in Fig. 2. A frequency-doubled, Nd:YAG-pumped dye laser provided the ultraviolet laser radiation for excitation of the OH molecule. The beam (8-ns pulse duration, 0.3-cm^{-1} line width) was used to pump the $Q_1(8)$ line of the (1,0) band of the OH $A^2\Sigma$ - $X^2\Pi$ electronic transition at 283.556 nm. Excitation from the N"=8 level was selected to minimize the temperature sensitivity of the fractional population within the absorbing level. The laser-pumped $Q_1(8)$ line has a population fraction that varies by only 10 percent over the temperature range 1000 K to 2300 K. The OH fluorescence signal was collected using a 105-mm (4.13 in) focal length, f/4.5 UV Nikkor lens, passed through a Schott WG305 colored glass filter, and focused onto an intensified CCD camera. The intensifier was gated for 400 ns, encompassing the 8-ns laser pulse, to minimize the effects of flame luminescence and background light. The camera was operated in a 512 x 512-pixel format. With a magnification of 0.15, each image provides a field-of-view of 81.9 mm x 81.9 mm (3.2 in x 3.2 in) with a spatial resolution of 160 μm/pixel (0.006 in/pixel).

The collimated laser sheet for the OH fluorescence was formed by a cylindrical/spherical lens combination. The spherical lens both collimated the expanding laser sheet and reduced the sheet thickness to approximately 200 μm (0.008 in) in the imaged area. An aperture located after the spherical lens was used to pass only the middle 50% of the sheet into the burner, thus minimizing variations in laser power across the sheet. The resulting laser power variation was less than 40 percent, which minimizes the corrections for laser sheet nonuniformities as described below. For this laser sheet configuration, a laser power of about 9 mJ/pulse was used. This power level provides an average spectral power density within the linear fluorescence regime where the fluorescence signal is a linear function of laser power and depends on the collisional quenching rate. The linearity of the fluorescence signal with laser power was verified experimentally.

The collisional quenching rate term is a function of temperature, pressure, and gas composition, which are typically not known. To establish the relationship between the fluorescence signal intensity and the OH concentration, one-dimensional, premixed flame calculations (Kee et al., 1985) were carried out over a range of hydrogen/methane/air mixtures to quantify corrections for quenching and ground state population fraction. Corrections were calculated for rotational levels of N"=6 and N"=8 and for hydrogen dilution levels up to 20%. It was concluded that linear LIF could be used to measure the OH mole fraction to within 10% without corrections for quenching and population fraction. Given the modest errors in the relative OH levels, the visualizations are expected to be fully representative of the actual flame structure.

Each OH image was normalized by the measured laser sheet intensity distribution and corrected for variations in pulse energy on a shot-by-shot basis. A laser sheet profiler was developed to measure the laser sheet intensity distribution. The sheet intensity distribution was obtained by using a thin quartz beam splitter to reflect a small percentage (~4%) of the incident laser sheet onto a WG305 Schott glass filter. The fluorescence from the filter glass was imaged onto one edge of the CCD camera array that recorded the OH image. Thus the laser sheet intensity distribution was recorded on the same image as the OH fluorescence signal. It was further found that the spatially-integrated laser sheet profiles recorded on the image provided a good measure of the total laser energy for each shot. Thus each image could be corrected for laser sheet intensity distribution and laser energy, on a shot-by-shot basis. Corrections were made to the images for variations in camera pixel sensitivity (flatfield) and background scattered light. Under the current flame conditions, with the pumping and detection scheme used, the OH fluorescence signal can be interpreted as the OH mole fraction to within 20 percent.

Acetone Fluorescence Imaging

Laser-induced fluorescence of acetone was used as a tracer for the fuel. Acetone was seeded directly into the fuel flow using an aerosol generator. Since the acetone absorption spectrum is continuous over the wavelength range of 240 to 320 nm, the same laser excitation wavelength of 283.553 nm was used to excite fluorescence from the acetone. This wavelength is to the long side of the peak excitation wavelength at 275 nm, but with 9 mJ of laser power, the fluorescence signal was sufficient to provide a good signal. The detection system for the acetone fluorescence was identical to that used for the OH fluorescence. As discussed by Clemens and Paul (1995), since the fluorescence signal from acetone is largely independent of its collisional environment, the fluorescence signal is proportional to the acetone number density. One problem with the use of acetone is that since it rapidly pyrolizes at temperatures above 1200K, acetone will not survive in the high temperature flame zone, and will also likely disappear when mixed with hot combustion products. For this reason, the mixing measurements described in the following section were limited to nonreacting flow conditions. In addition, hydrogen could not be used with the current aerosol generator due to safety concerns. The hydrogen fuel injected through the small diameter opposing holes in the sides of the reactant channels was therefore replaced with air. The acetone seeding levels in the air were typically 3,000 ppm by volume.

Experimental Results

The flame stability characteristics were determined for the burner over a range of operating conditions. Since it was found early that under some operating conditions the burner confinement section began to rapidly overheat, initial studies were carried out in the burner without the windowed confinement section in place to minimize potential damage of the confinement section. Once a better understanding of the unconfined burner characteristics was obtained, further characterization of the flame was done with the confinement section in place. The main parameters studied were the inlet flow rate, or velocity, and the overall fuel/air equivalence ratio, ϕ. The inlet flow velocity, u, is related to the inlet flow rate by the equation:

$$u = Q_{in} / A_{in} \qquad (1)$$

where Q_{in} is the inlet volumetric flow rate and A_{in} is the total inlet area of 3.194 cm^2 (0.495 in^2). In all results described below, the inlet flow rate used is the total combined flow rate of air and fuel. The inlet flow velocity is based on this total flow rate and the total area of the nine 6.72-mm (0.265 in) diameter inlet flow channels. It was determined that flame flashback was easier to prevent while operating conditions were varied if a fuel mixture consisting of H_2 and CH_4 was used. Thus, an additional parameter, the mole fraction of H_2 in the fuel mixture, n_{H2}=moles H_2/(moles H_2 + moles CH_4), was added as a burner variable. This provided control over the flame speed, which is significantly reduced by the addition of small amounts of CH_4. The addition of this variable also provides the possibility of studying the effect of flame speed variations on the flame characteristics and evaluating potential improvements in stability under conditions where hydrogen is the primary fuel component.

Unconfined Flame Configuration

A stability map for the unconfined flame is shown in Fig. 3 for a value of n_{H2} =0.9. Note that only fuel lean conditions were studied since fuel lean combustion is the likely method of NO_X control in future gas turbine combustors. The measurements in Fig. 3 were obtained by igniting the flame at near stoichiometric conditions (ϕ =0.9) and then, with a constant total (fuel+air) flow rate (or inlet velocity), decreasing the fuel/air ratio. Over the range of velocities considered, three flame regimes could be easily identified. The points labeled a, b and c at u=30 m/s (98.4 ft/s) correspond to a typical sequence of flames in which the fuel/air ratio is decreased while maintaining a constant inlet velocity. Figure 4 shows photographs of the flame emission corresponding to these flames. At the highest equivalence ratios (Fig. 4a) flames are stabilized above each of the nine-reactant inlet channels and are about equal in size. Each flame is lifted and stabilized about 6 mm (0.236 in) above the inlet plane. As the fuel/air ratio is decreased (Fig. 4b) the flame enters a new regime in which the outer flames (i.e. those flames stabilized above all but the central reactant inlet channel) decrease in size, or shrink, relative to the central flame and are stabilized farther downstream from the inlet plane. Since equal flow rates are maintained through each of the channels, and the equivalence ratios are the same, it can be speculated that these observations are related to entrainment of ambient room air into the outer jets. This added air effectively reduces the fuel/air ratio in the individual jets, which has the effect of decreasing the flame velocity, increasing the liftoff height and reducing the reaction intensity, which is manifested in reduced emission intensity from these outer flames. Little ambient air is expected to be entrained into the central jet or the region immediately around it. As the fuel/air ratio is further reduced (Fig. 4c), both the central and outer flames move farther downstream and flame emission continues to decrease until the flame eventually blows out. The solid line in Fig. 3 indicates measured conditions where total flame extinction occurs.

Planar Laser-Induced Fluorescence (PLIF) images of the OH signal are shown in Fig. 5 for each of the three flow conditions of Fig. 4. As noted above, the OH signal can be interpreted as the OH mole fraction to within about 20 percent. Further, these images are representative of the instantaneous OH mole fraction distributions since the laser pulse duration of 8 nsec is sufficiently short relative to the flow time scales to effectively “freeze” the motion of the flow. Note that the 2 Hz framing rate of the camera is to slow to follow the temporal evolution of the flow, so the images presented are typical single shot images showing the instantaneous OH distribution at random times. Figure 5a shows four images corresponding to different laser shots for the flame pictured in Fig. 4a at an equivalence ratio of 0.90. Note that the cross-hatched areas along the bottom of the images indicate locations where a solid surface exists between the inlet channels while breaks between the cross-hatched areas indicate channel openings where reactants enter the combustion chamber. The upstream edge of the high OH region is very irregular and probably reflects variations in the local velocity, which contort the flame surface. The OH is nearly uniform throughout large regions of the downstream flame, with locally high concentration regions forming thin filaments that extend throughout the high OH region.

Two lower intensity but still visible OH regions extend upstream from the main flame zone to the two solid walls located adjacent to the central channel opening. (Note that blocking of the camera view results in no signal in the region extending several millimeters above the two solid walls. The actual OH signal extends up to the actual wall surfaces). Analogous to the flow field produced downstream of a centerbody, it is likely that recirculation zones are formed between the inlet flow channels and downstream of the solid walls in the plane of the laser light sheet. Velocity field measurements downstream of a centerbody show a recirculation zone that extends one to two centerbody diameters downstream, followed by a wake region with a velocity deficit near the centerline (Taylor and Whitelaw, 1984). Recent calculations carried out for the present flow geometry using the NASA National Combustion Code (Marek, 2002) confirm the presence of high temperature recirculation zones adjacent to the reactant inlet flow. These recirculation and wake zones provide low reverse-velocity regions that are favorable to upstream flame propagation from the larger downstream flame zone. The OH levels in these regions are lower than in the downstream flame zone and likely reflect the relatively long residence times in the recirculation zone, which allow the OH concentration to relax toward equilibrium values. As shown in Fig. 4a, visible flame emission is very weak in these regions.

The OH PLIF images in Fig. 5b for an equivalence ratio of 0.74 correspond to the flame pictured in Fig. 4b. Generally, the OH images reveal features similar to the OH images at the higher equivalence ratio of 0.90. Noteworthy is the vertical location where OH is first observed at outer radial locations, which has moved farther downstream. These observations are consistent with the visible flame emission, which shows the outer flames decrease in size and stabilize farther downstream as the equivalence ratio is reduced. At the lowest equivalence ratio of 0.68 (Fig. 5c), no OH is seen extending upstream into the recirculation/wake regions and the outer flames are stabilized even farther downstream. As noted previously, these observations are likely due to excess air entrained into reactants entering from the outer channels, which results in a reactant mixture that is to lean to support combustion in these outer regions.

The effect of varying the H_2 content in the fuel mixture is shown in Fig. 6 where flame stability maps are shown for n_{H2}=0.8, 0.9 and 1.0 (pure hydrogen). Again, dashed lines indicate the transition from the equal flame regime to the shrinking flame regime, while solid lines indicate flame blowout conditions for each value of n_{H2}. The increase in hydrogen content from 80% to 100% results in a significant shift in flame blowout conditions to leaner fuel/air ratios. This shift is consistent with studies in the literature showing an increase in the lean flammability limits with the addition of small amounts (<40%) of hydrogen to methane (Wicksall, and Agrawal, 2001; Schefer et al., 2002) and verifies that H_2 addition significantly extends lean flame stability even at the higher percentages considered here. For example, at a velocity of 50 m/s (164 ft/s), increasing n_{H2} from 0.8 to 1.0 reduces the equivalence ratio at flame blowout from ϕ =0.86 to 0.58. Note that since the flame here is unconfined, the actual equivalence ratio at blowout is likely to be considerably less than that based on measured flow rates due to dilution of the reactant mixture by entrained air. Results for confined flames shown in the following section verify the effectiveness of H_2 addition at extending lean flame stability limits even at high values of n_{H2}.

Confined Flame Configuration

Flame stability was next characterized in flames with the quartz-windowed confinement section in place. Figure 7a shows blowout curves for values of n_{H2}=0.7, 0.8, 0.9 and 1.0. As with the unconfined case, flame blowout occurs at significantly leaner conditions as the percentage of H_2 is increased. Comparison with the unconfined blowout curves in Fig. 6 also shows that, for the same inlet velocity and hydrogen addition, blowout for the confined flames occurs at nearly half the equivalence ratio seen in the unconfined case. As noted above, it is likely that entrained air in the unconfined flame effectively reduces the equivalence ratio over that based on measured flow rates. Thus the actual equivalence ratios at blowout in Fig. 6 are much lower than indicated by the horizontal axis, which is based on the measured flow rates of fuel and air.

The flame blowout characteristics have been replotted in Fig. 7b. This presentation of the data better illustrates the effect of H_2 addition on the blowout velocity for a given value of equivalence ratio. Note that the points corresponding to n_{H2}=1.0 and ϕ =0.25 and 0.30 are based on an extrapolation of the linear blowout curve for n_{H2}=1.0 in Fig. 7a to higher velocities that were not accessible with the current flow system. It can be seen that for $n_{H2} < 0.9$ the increase in blowout velocity with n_{H2} for a fixed equivalence ratio is relatively gradual, while for $n_{H2} > 0.9$ the increase is more rapid. The reason for the more rapid increase at higher H_2 addition is not clear and needs further study.

As with the unconfined flames, different flame regimes can be identified with confinement. These more detailed regimes are shown in Fig. 8 for n_{H2}=0.8. The points labeled **a**, **b** and **c** at u=30 m/s (98.4 ft/s) correspond to each of the three flame regimes identified. Flame emission photographs corresponding to these flames are shown in Fig. 9. At the highest equivalence ratio of ϕ =0.6 in Fig. 9a, which corresponds to point **a** in Fig. 8, multiple stable lifted flames are observed. For each reactant channel, a separate flame can be identified, although the outer portions of the individual flames do overlap. The flame liftoff height is about 20 mm (0.8 in) above each reactant channel and the flame luminescence extends over a distance of about 43 mm (1.7 in). Each flame appears stable, with little axial or radial movement observed visually. Note that there is some temporal averaging due to the finite time response of the eye, so the instantaneous structure and location of the flames could vary significantly from what is observed visually. No flame luminescence is seen extending above the end of the confinement section, indicating a relatively short reaction zone. As the equivalence ratio is reduced to ϕ =0.4 in Fig. 9b, corresponding to point **b** in Fig. 8, a region of unsteady lifted flames is observed. While each reactant channel again has a separate flame associated with it, the vertical location of the flame oscillates at a frequency on the order of 1 or 2 Hz. Intermittently, individual flames can be seen to closely approach the reactant channel inlet and then move downstream. The noise level also increases in this regime, with the increased noise perhaps related to interactions between the incoming reactant flow and the flame when it is located upstream near the reactant inlet.

Further reductions in the equivalence ratio to ϕ =0.3 in Fig. 9c, corresponding to point **c** in Fig. 8, result in each flame moving upstream and attaching at the reactant channel inlet. The typical visible flame length under these conditions is about 40 mm (1.6 in). These flames appear quite stable with little movement in their visually-averaged location. Further reductions in equivalence ratio lead to the sudden simultaneous blowout of the individual flames. It is interesting in Fig. 8 that these three flame regimes are readily apparent at lower inlet velocities. However, at inlet velocities above about 60 m/s (297 ft/s), the flames no longer attach to the reactant inlet and only the stable and unstable lifted flame regimes are observed.

OH PLIF images corresponding to the three flames of Fig. 9 for n_{H2}=0.8 are presented in Fig. 10. Four instantaneous images from different laser shots are shown at each flame condition to illustrate the time-varying characteristics of the flow. The images in Fig. 10a are for the highest equivalence ratio of 0.60 and clearly show that the flame is lifted between 15 mm (0.59 in) to nearly 30 mm (1.18 in) above the inlet plane. This liftoff height oscillates from shot-to-shot. As with the unconfined flames, the upstream edge of the flame (as indicated by the high OH region) is very irregular and probably reflects variations in the local velocity, which contort the flame surface. The OH is uniform throughout large regions of the downstream flame, with the highest concentration regions existing along the upstream edges of the high OH region. These high concentration regions correspond to what could be considered as the primary flame zone, which is located between the unburned reactants and the hot product gases. Recent OH PLIF measurements in rod stabilized, premixed CH_4/air flames also show peak OH levels in the primary flame zone along the interface between incoming reactants and hot combustion product gases, with a subsequent decrease downstream as radical recombination reactions lower the OH levels (Nguyen and Paul, 1996). More gradual variations in OH are seen throughout the flame in downstream regions, with only a few breaks or holes seen in the OH surface.

The OH images seen in Fig. 10b for ϕ =0.40 again show a flame that is lifted, but also present a considerably more broken, or intermittent, flame surface. This likely reflects the greater unsteadiness observed visually in this flame, with the flame stabilization location, or liftoff height oscillating in the vertical direction. This flame was also considerably more noisy. The OH images confirm large oscillations in the liftoff height as the location of the first appearance of OH varies between as little as 5 mm (0.20 in) to nearly 30 mm (1.18 in) downstream.

At the leanest equivalence ratio of ϕ =0.30 the flame is visually stable and attached. The corresponding OH images in Fig. 10c confirm this, with the high OH region extending upstream to the solid surfaces adjacent to the reactant inlet channels. As discussed in the unconfined case, these upstream regions are likely lower-velocity recirculation zone and wake regions that allow upstream flame stabilization. A nonreacting region typically extending between 30 mm (1.18 in) and 50 mm (1.97 in) downstream of the inlet plane is seen above each of the reactant inlet channels. This region can be characterized as a high velocity jet of unburned reactants where the velocity is too high to allow the flame to stabilize. It can also be seen that the highest OH concentration is along the interface between the nonreacting jet region and the recirculation/wake region consisting of hot product gases. Again the high OH region exhibits a more continuous sheet-like appearance rather the largely broken surface seen in Fig. 10b.

Detailed flame regime maps were obtained for n_{H2}=0.7, 0.9 and 1.0 to further explore these observed flame regimes. These are shown in Figs. 11 through 13, respectively. For n_{H2}=0.7, unstable and stable lifted flames were observed over the velocity range considered, but no attached flames were found. At both n_{H2}=0.8 and 0.9 (Figs. 8 and 12, respectively), a lower velocity region exists where flames attached to the reactant channel inlets are observed, with the maximum velocity at which an attached flame is seen increasing with increasing n_{H2}. The detailed flame regime map for n_{H2}=1.0 in Fig. 13 exhibits somewhat different behavior. Over the velocity range investigated all flames were attached to the individual reactant inlet channels. No lifted flames were observed. This behavior is consistent with the increase in maximum velocity for the attached flame regime as n_{H2} is increased. Thus, an unstable lifted flame regime may exist at velocities greater than the 120 m/s (394 ft/s) attained in the experiment. The points labeled a and b in Fig. 13 correspond to the two flame luminosity photographs shown in Fig.14. Both of these flames are in the multiple stable attached flame regime, with the flame in Fig. 14 a) corresponding to conditions nearer to flame blowout. Visually, as blowout is approached, the individual flames become shorter and less luminous.

Note also the single point for n_{H2}=0.9 in Fig. 12 at u=30 m/s (98 ft/s) and ϕ =0.6 labeled “flashback”.At these operating conditions the flame appeared to propagate upstream and stabilize inside the premixed reactant inlet channel. This resulted in a very loud, high-pitched, noisy flame. For other values of n_{H2} it is likely that similar flashback-modes of operation exist at sufficiently high equivalence ratios and low inlet velocities. This behavior is due to the tradeoff between increasing flame speed as ϕ and n_{H2} are increased and the lower inlet velocity, which allows the flame to propagate upstream into the premixed inlet channel. Because of safety concerns, these operating conditions were subsequently avoided and only one flashback point is indicated in Fig. 12.

Figure 15 shows PLIF images of the OH distribution corresponding to the flames pictured in Fig. 14. The four images in Fig. 15a are for n_{H2}=1.0, u=90 m/s (295 ft/s) and ϕ =0.33 (point a). Similar to Fig. 10c, the flame is attached to the burner surface, with the high OH region extending upstream to the solid surfaces adjacent to the reactant inlet channels. A nonreacting, high velocity jet region typically extending between 30 mm (1.18 in) and 50 mm (1.97 in) downstream of the inlet plane is also seen above the reactant inlet channel in the center of the images. The highest OH concentrations are found along the vertical interfaces between the nonreacting jet region and the reacting recirculation/wake region. The OH images in Fig. 15b for n_{H2}=1.0, u=70 m/s (230 ft/s) and ϕ =0.15 (point b) are similar with the exception that the nonreacting jet region does not extend as far downstream as in Fig 15a. This observation would seems to confirm the speculation that this region can be characterized as a high velocity jet where the velocity is too high to allow the flame to stabilize. At the lower inlet velocity in Fig. 15b, the jet velocity decays more rapidly to a velocity at which the flame can stabilize.

Figure 13 also shows that as the equivalence ratio is increased a regime exists in which, while the flames remain attached, the combustor also becomes quite noisy. This noise consists of a loud, high-pitched whistle in addition to the lower frequency noise associated the high flow rate of reactants out of the inlet nozzle. It is believed that this noise is associated with interactions between the reactant flow in the inlet channels and the flames, which are attached to the channel inlets and, perhaps, burns up into the holes due to the increase in flame velocity with increased equivalence ratio.

Shown in Fig. 16 is a close-up photograph of the flame in Fig. 14a). The velocity of 90 m/s (295 ft/s), equivalence ratio of 0.33 and n_{H2}=1.0 are close to the nominal design conditions for the present burner (u=122 m/s (402 ft/s), ϕ=0.29). Visual observation shows that the luminous flame zone extends up the reactant channel exit plane. Whether the flame extends further into the channel is not clear. Inspection of the inner channel walls appeared to show some metal discoloration, as would be expected if sufficient heating by the flame had occurred. It is also interesting that the flame luminescence is not uniform around the circumference of each flame, but appears to have multiple (three) regions of high luminescence extending a fair distance downstream, separated by regions of lower luminescence. This behavior may indicate nonuniform mixing of the radially injected H_2 with the air. PLIF images of OH and acetone (for a fuel marker) would help to quantify the mixing provided by the current burner design.

Mixing Behavior using Acetone PLIF Imaging

As described above, the hydrogen flow through the small-diameter jets located in the reactant flow channel walls was replaced by air and low levels of acetone were seeded into the air flow to provide a tracer for the "fuel" and its subsequent mixing with primary air flowing in the main inlet channels. Acetone PLIF images were obtained for a fixed flow rate of "fuel", that was determined by the operation of the acetone atomizer to be 65.6 slm (2.32 ft^3/m). Given the 18 "fuel" injection holes, each with a diameter of 0.0906 cm (0.0357 in), this flow rate corresponds to a velocity exiting each hole of 98 m/s (321 ft/s). Measurements were obtained for primary air velocities of 50 m/s (164 ft/s), 40 m/s (131 ft/s), 30 m/s (98.4 ft/s) and 20 m/s (66 ft/s). We will assume that the relevant parameter controlling mixing of the fuel jet into the cross-flowing primary air stream is the ratio of the fuel jet to primary air momentum ratio, J. This is defined as:

$$J = (\rho_{fuel} * u^2_{fuel}) / (\rho_{air} * u^2_{air}) \qquad (2)$$

where ρ_{fuel} and ρ_{air} are the density of the fuel and air, respectively, and u_{fuel} and u_{air} are the velocities of the fuel jets and air channels. The above primary air velocities thus give values for J of 3.82, 5.97, 10.61 and 23.9, respectively.

Acetone PLIF images (single shot) are shown in Fig. 17 for these flow conditions. Note that the signal level is linearly proportional to the acetone concentration so that the lowest signal (dark blue or black) corresponds to unmixed primary air (no acetone) while the highest (red) signal corresponds to the original acetone level in unmixed "fuel" prior to injection into the primary air channels. Unlike the fuel in the reacting flows, which is consumed due to combustion, acetone is not consumed here so variations of the acetone signal reflect only variations in mixing. At the lowest J of 3.82 (Fig. 17a) it is clear that the injected "fuel" has not mixed well with the primary air since considerable variation in acetone signal exists throughout the flow. As the momentum ratio is increased to 5.97 and 10.61, some variation in acetone signal is still apparent but shows less variation than at the highest momentum ratio. Finally, at J =23.9 (Fig. 17d) the signal variation is quite uniform throughout the flow indicating good mixing between the “fuel” and primary air. Assuming that sufficient penetration of the fuel jet into the cross-flowing air channel is required for good mixing, then it seems reasonable that increasing the fuel-jet momentum relative to the air momentum should result in greater fuel-jet penetration and improved mixing.

It is of interest to relate the mixing measurements obtained in the nonreacting flow using air as the “fuel” to the nominal burner design conditions of n_{H2}=1.0, u=122 m/s (402 ft/s) and ϕ =0.29. These values were calculated for the nominal burner design operating condition and for the acetone measurement conditions and are summarized in Table 1. The fuel and air flow rates in Table 1 are for a single fuel injection hole and a single air channel.

Note from Fig. 17 that as the momentum ratio decreases the mixing becomes less complete and that the momentum ratio for the nominal design condition of 0.715 is lower than the range of momentum ratios measured in the acetone tests. Assuming the observed trend continues it then appears that mixing of fuel and air at the nominal design condition is also unlikely to be good. Based on these results a design change that increases J could provide better mixing.

Table 1. Conditions for single fuel injection hole and air channel.

Conditions	Q_{air}	m_{air}	u_{air}	Q_{fuel}	m_{fuel}	u_{fuel}	ρ_{fuel}/ρ_{ai}	J
Nominal: u=122 m/s (402 ft/s), ϕ=0.29, n_{H2}=1.0	234 slm (8.2 ft^3/m	5.0 g/s (0.010 lb/s)	109.7m/s (360 ft/s)	13.4 slm (0.47ft^3/m)	0.0212 g/s (0.000047 lb/s)	348 m/s (1142 ft/s)	0.071	0.715
Acetone	106.0 slm (3.7 ft^3/m	2.131 g/s (0.0047 lb/s)	50.0 m/s (164ft/s)	3.64 slm (0.13 ft^3/m)	0.073 g/s (0.00016 lb/s)	97.7 m/s (320 ft/s)	1.0	3.82
Acetone	85.3 slm (3.0 ft^3/m	1.715 g/s (0.0038 lb/s)	40.0 m/s (131 f/s)	3.64 slm (0.13 ft^3/m)	0.073 g/s (0.00016 lb/s)	97.7 m/s (320 ft/s)	1.0	5.97
Acetone	64.0 slm (2.2 ft^3/m	1.286 g/s (0.0028 lb/s)	30.0 m/s (98.4 f/s)	3.64 slm (0.13 ft^3/m)	0.073 g/s (0.00016 lb/s)	97.7 m/s (320 ft/s)	1.0	10.61
Acetone	42.7 slm (1.5 ft^3/m	0.858 g/s (0.0019 lb/s)	20.0 m/s (66 f/s)	3.64 slm (0.13 ft^3/m)	0.073 g/s (0.00016 lb/s)	97.7 m/s (320 ft/s)	1.0	23.9

Summary

The stability and flame characteristics of a novel premixed, hydrogen-fueled burner were studied. In addition to pure hydrogen and air, mixtures of hydrogen-blended methane and air were studied. Depending on the inlet flow variables, flame regimes were identified that included both lifted and attached flames. Conditions under which these varying flames were observed were mapped out, as were those conditions at which the flame was extinguished. Generally, the leanest stability limits were found with pure H_2 flames, while the addition of methane required a higher equivalence ratio to maintain a stable flame. At the nominal design conditions for the burner, stable attached flames were achieved. OH PLIF images verified the presence of lifted unattached flames and flame that typically were attached to the burner surface and stabilized in the recirculation/wake region produced by the flow downstream of the solid walls located between reactant inlet channels. Acetone was used as a fuel tracer to evaluate the degree of mixing between the incoming fuel jets and the primary air. These tests were carried out in a nonreacting flow with the fuel replaced with acetone-seeded air. It was found that with low values of fuel-jet to primary air momentum ratios mixing was not very good, while for higher values of the momentum ratio uniform mixing of the fuel and air was achieved.

Possible Future Work

1. The PLIF measurements of the acetone were used to characterize the mixing process under nonreacting conditions and with the H_2 replaced with air, but at fuel/air momentum ratios higher than those near the nominal design conditions. These measurements could be extended to the expected nominal design flow rates.
2. Particle Imaging Velocimetry (PIV) measurements could allow us to characterize the combustion flow dynamics and quantify the role of fluid dynamics in flame stability.

Acknowledgements

This research was supported by the U. S. Department of Energy, Office of Energy Efficiency and Renewable Energy, Hydrogen, Fuel Cells and Infrastructure Technologies Program. The experiments were conducted at the Sandia Combustion Research Facility in laboratories supported by the U. S. Department of Energy, Office of Basic Energy Sciences, Chemical Sciences.

Bibliography

Anderson, D. N., "Effect of Hydrogen Injection on Stability and Emissions of an Experimental Premixed Prevaporized Propane Burner," NASA Technical Memorandum NASA TM X-3301, 1975.

Anderson, D. N., "Emissions of Oxides of Nitrogen From an Experimental Premixed-Hydrogen Burner," NASA Technical Memorandum NASA TM X-3393, 1976.

Barlow, R. S. and Collignon, A., "Linear LIF Measurements of OH in Nonpremixed Methane-Air Flames: When Quenching Corrections Unnecessary," Presented at AIAA Twenty-Ninth Aerospace Sciences Meeting, Reno, NV, January 7-10, paper No. AIAA 91-0179, 1991.

Bell, S. R. and Gupta, M., "Extension of the Lean Operating Limit for Natural Gas Fueling of a Spark Ignited Engine Using Hydrogen Blending,"*Combust. Sci. Technol*. **123**: 23-47 (1997).

Clayton, R. M., "Reduction of Gaseous Pollutant Emissions from Gas Turbine Combustors Using Hydrogen-Enriched Jet Fuel – A Progress Report," NASA TM 22-790, 1976.

Clemens, N. T. and Paul, P. H., "Effects of Heat Release on the Near Field Flow Structure of Hydrogen Jet Diffusion Flames, " Combust. Flame **102**: 271-284 (1995).

Gauducheau, J. L., Denet, B. and Searby, G., *Combust. Sci. Technol*. **137**: 81-99 (1998).

Kee, R. J., Rupley, F. M., Miller, J. A., Coltrin, M. E., Grcar, J. F., Meeks, E., Moffat, H. K. Lutz, A. E., Dixon-Lewis, G., Smooke, M. D., Warnatz, J., Evans, G. H., Larson, R. S., Mitchell, R. E., Petzold, L. R., Reynolds, W. C., Caracotsios, M., Stewart, W. E., and Glarborg, P., Chemkin Collection, Release 3.5, Reaction Design, Inc., San Diego, CA (1999).

Larsen, J. F. and Wallace, J. S., *J. Engineering for Gas Turbines and Power* **119**: 218-226 (1997).

Marek, C. J. (personal communication), 2002.

Meyers, D. P. and Kubesh, J. T., *J. Engineering for Gas Turbines and Power* **119**: 243-249 (1997).

Morris, J. D., Symonds, R. A., Ballard, F. L. and Banti, A., ASME Paper 98-GT-359 (1998).

Nguyen, Q. and Paul, P. H., *Twenty Sixth Symposium (International) on Combustion*, The Combustion Institute, Pittsburgh, 1996, p. 357-364.

Phillips, J. N. and Roby, R. J., ASME Paper 99-GT-115 (1999).

Schefer, R. W., Wicksall, D. M. and Agrawal, A. J., “Combustion of Hydrogen-Enriched Methane in a Lean Premixed Swirl-Stabilized Burner,” Proceedings of the Twenty-Ninth Symposium (International) on Combustion, Sapporo, Japan, July 21-26, 2002.

Wicksall, D. M. and Agrawal, A. J., “Lean Premixed Combustion of Hydrogen-Enriched Natural Gas,” Presented at the 2000 Technical Meeting of the Central States Section/The Combustion Institute, 2000.

Appendix I

Presented in Table A1 are the flow rates corresponding to the data presented in Figures 1 through 15 for the reacting flows. No flow rates from the flame stability maps are included. Note that the order of the cases in Table A1 corresponds to the approximate order in which flame photographs and OH PLIF images are presented in the paper.. The mass flow rates are the total flow rates for the burner (all nine air channels and 18 fuel injection holes). The velocity, u, is based on the total volumetric flow rate (fuel plus air) and the total inlet channel area using Eqn. (1). The Reynolds number, Re, is based on the single air channel inlet diameter and velocity and assumes the reactant mixture is at atmospheric pressure and room temperature of 293 K. Mass flow rates for the acetone mixing studies are given in Table 1 and are the flow rates of fuel and air through either a single fuel injection hole or a single air channel. This was done on a single channel/hole basis to facilitate comparisons with model calculations for a turbulent jet into cross flow.

Table A1. Conditions for burner.

Case	u	n_{H2}	ϕ	Re	m_{CH4}	m_{H2}	m_{air}
1	30 m/s (98.4 ft/s)	0.9	0.9	11456	0.1428 g/s (0.315x10^{-3} lb/s)	0.1752 g/s (0.386x10^{-3} lb/s)	8.96 g/s (19.7x10^{-3} lb/s)
2	30 m/s (98.4 ft/s)	0.9	0.74	11619	0.1223 g/s (0.270x10^{-3} lb/s)	0.1501 g/s (0.331x10^{-3} lb/s)	9.34 g/s (20.6x10^{-3} lb/s)
3	30 m/s (98.4 ft/s)	0.9	0.68	11683	0.1142 g/s (0.252x10^{-3} lb/s)	0.1401 g/s (0.309x10^{-3} lb/s)	9.49 g/s (20.9x10^{-3} lb/s)
4	30 m/s (98.4 ft/s)	0.8	0.6	11998	0.1725 g/s (0.380x10^{-3} lb/s)	0.0941 g/s (0.208x10^{-3} lb/s)	10.00 g/s (22.0x10^{-3} lb/s)
5	30 m/s (98.4 ft/s)	0.8	0.4	12176	0.1204 g/s (0.265x10^{-3} lb/s)	0.0657 g/s (0.145x10^{-3} lb/s)	10.48 g/s (23.1x10^{-3} lb/s)
6	30 m/s (98.4 ft/s)	0.8	0.3	12271	0.9254 g/s (0.204x10^{-3} lb/s)	0.0505 g/s (0.111x10^{-3} lb/s)	10.73 g/s (023.6x10^{-3} lb/s)
7	90 m/s (295 ft/s)	1.0	0.33	35670	0.0	0.3156 g/s (0.696x10^{-3} lb/s)	30.50 g/s (67.2x10^{-3} lb/s)
8	70 m/s (230 ft/s)	1.0	0.15	28565	0.0	0.1195 g/s (0.263x10^{-3} lb/s)	25.41 g/s (56.0x10^{-3} lb/s)

Appendix II

Calculations were carried out using the Chemkin equilibrium code (Kee et al., 1999) to determine the effect of hydrogen content on the adiabatic flame temperature and the OH mole fraction. Shown in Fig. A1 is the variation in the adiabatic flame temperature, T_{ad},, with equivalence ratio for various mixtures of hydrogen and methane as the fuel. The calculations were carried out at constant enthalpy and atmospheric pressure As expected, the flame temperature increases monotonically with equivalence ratio over the range of fuel-lean mixtures shown. Note that for hydrogen addition up to 40% (n_{H2}=0.4), the increase in flame temperature with increasing n_{H2} is nearly negligible. For example, over the range of equivalence ratios shown, the increase in T_{ad} with up to 40% hydrogen addition never exceeds1.7%. Greater hydrogen addition results in a larger temperature increase, reaching a maximum increase (over the value for no hydrogen addition) of about 11% for pure H_2 at ϕ = 0.3.

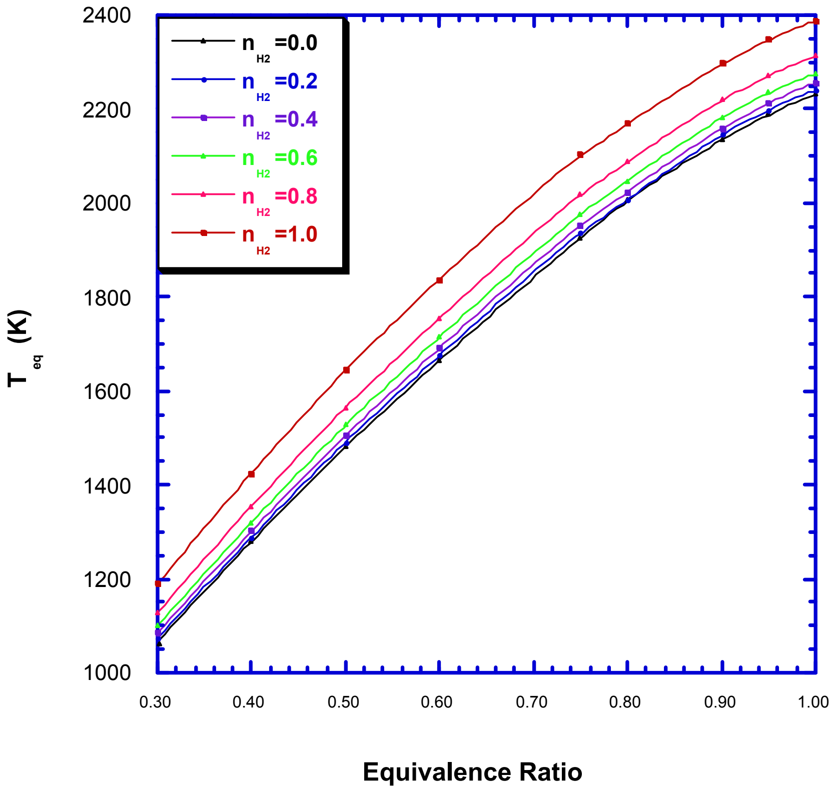

Fig. A1. Calculated adiabatic flame temperatures as a function of equivalence ratio and fuel hydrogen content.

Figure A2 shows the calculated variation in equilibrium OH mole fraction with equivalence ratio for various mixtures of hydrogen and methane as the fuel. Again, results are shown for values of n_{H2} varying from 0 (pure methane) to 1.0 (pure hydrogen). The equilibrium OH mole fraction increases rapidly with equivalence ratio to a maximum on the lean side of stoichiometric at ϕ =0.95 before decreasing as the reactant mixture becomes fuel rich. The maximum increase in OH mole fraction with up to 40% hydrogen addition is nearly 50%, while the maximum increase with pure hydrogen can be up to a factor of four at the leanest equivalence ratios. The increase in OH mole fraction with equivalence ratio and hydrogen addition is likely due to the higher flame temperature as these variables are increased, which drives the equilibrium composition toward higher radical concentrations.

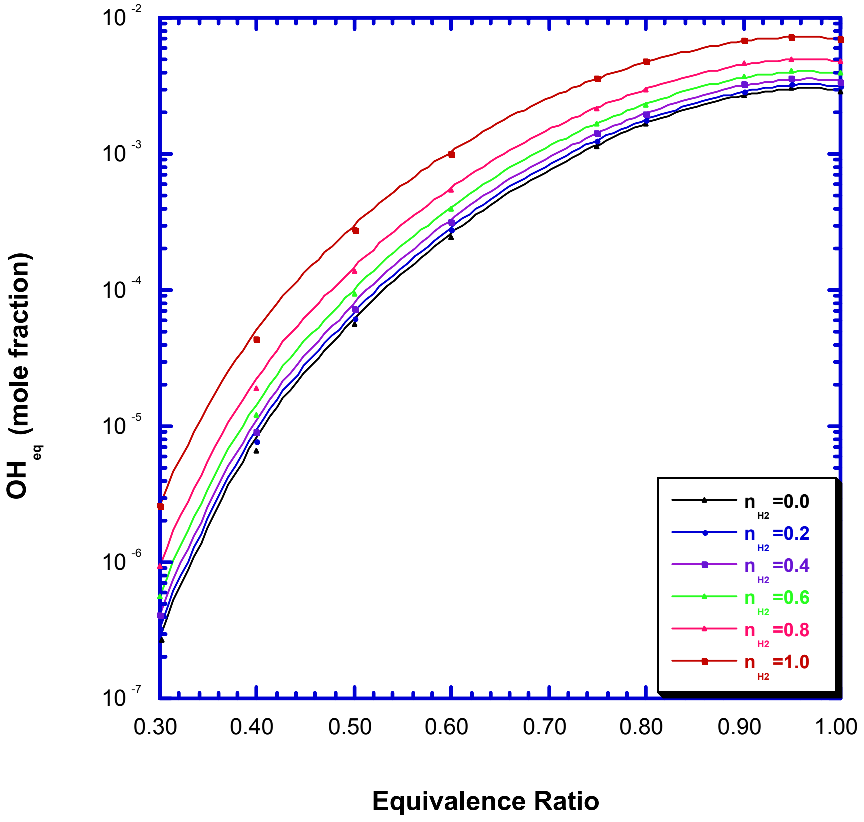

Fig. A2. Calculated OH mole fraction as a function of equivalence ratio and fuel hydrogen content.

The results presented in Figs. A1 and A2 have been combined in Fig. A3 to show the variation in OH equilibrium mole fraction with calculated adiabatic flame temperature. The plot shows a good collapse of the data for a range of n_{H2}, indiacting that the equilibrium OH is primarily determined by flame temperature and only secondarily by the H_2 addition.

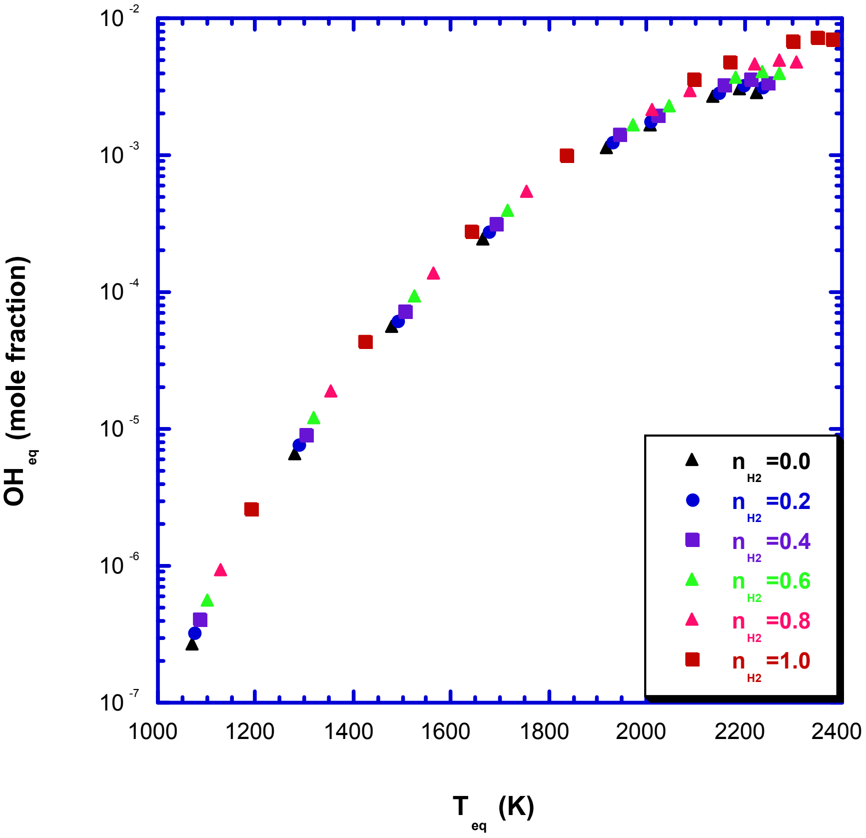

Fig. A3. Calculated OH mole fraction as a function of adiabatic flame temperature.

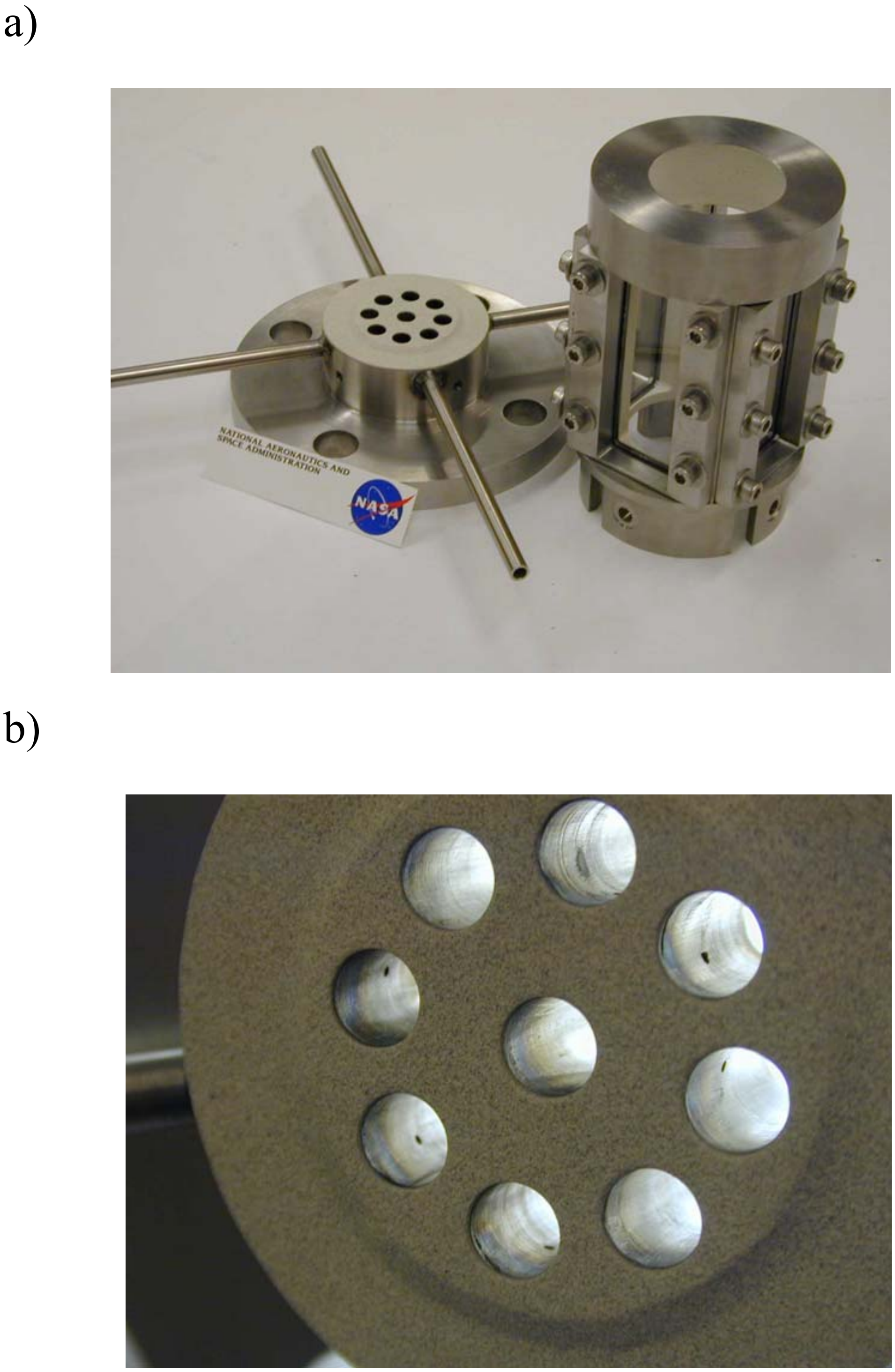

Fig. 1. NASA burner. a) Reactant inlet manifold (left) and windowed burner confinement section (right). b) Close up view of reactant inlet and H_2 radial injection holes.

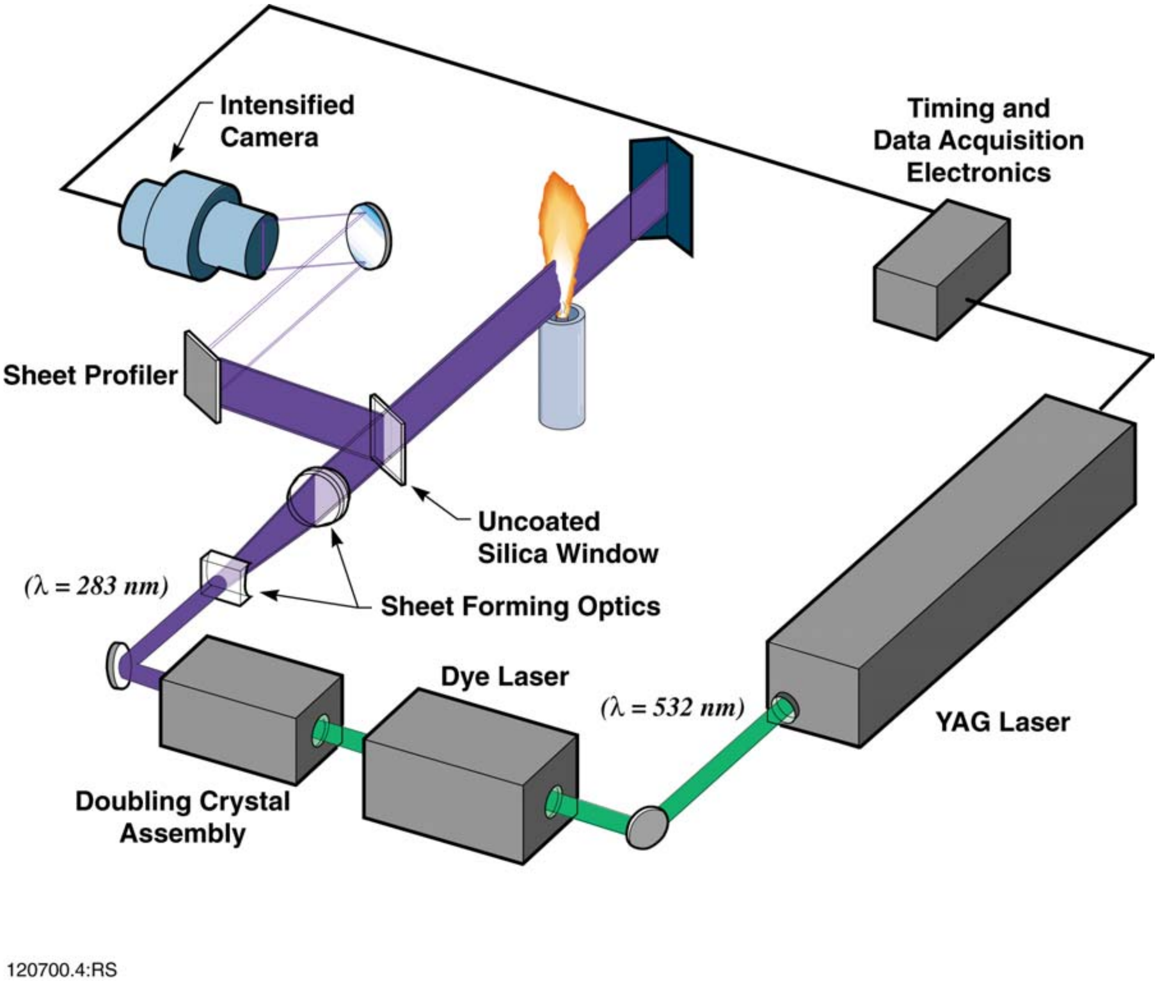

Fig. 2. Schematic of OH PLIF imaging system.

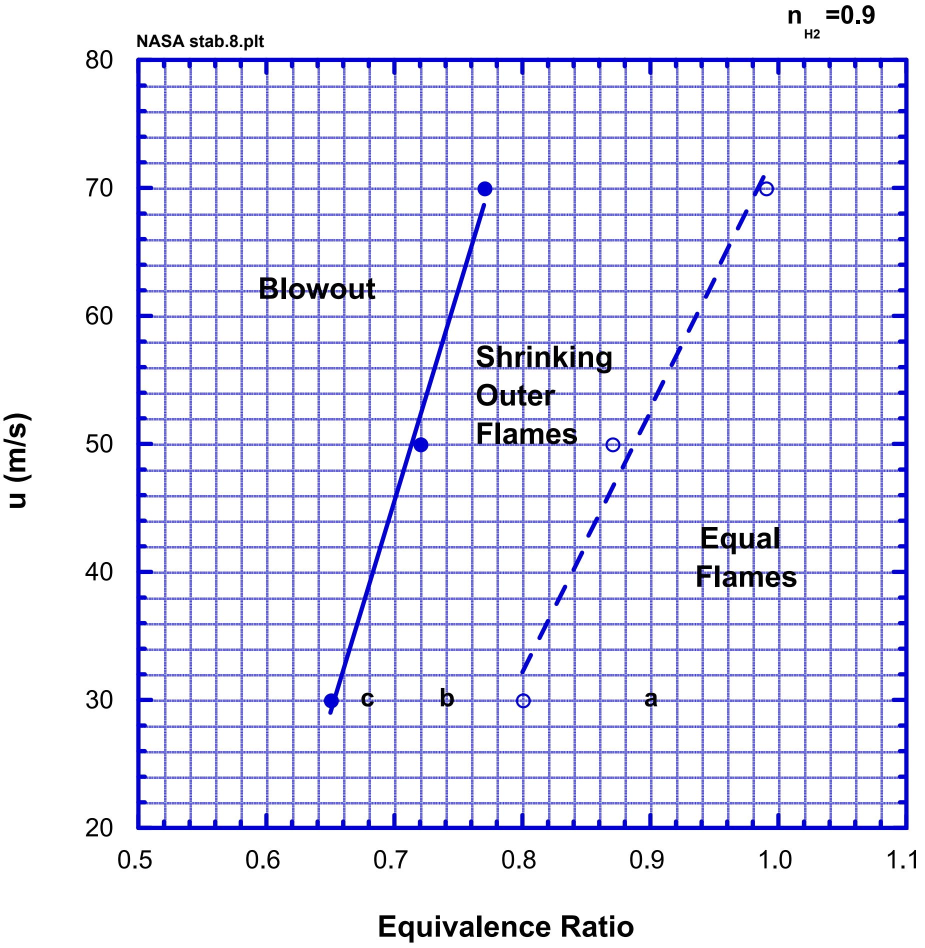

Fig. 3. Burner flame regime and stability map for n_{H2}=0.9. Unconfined flame.

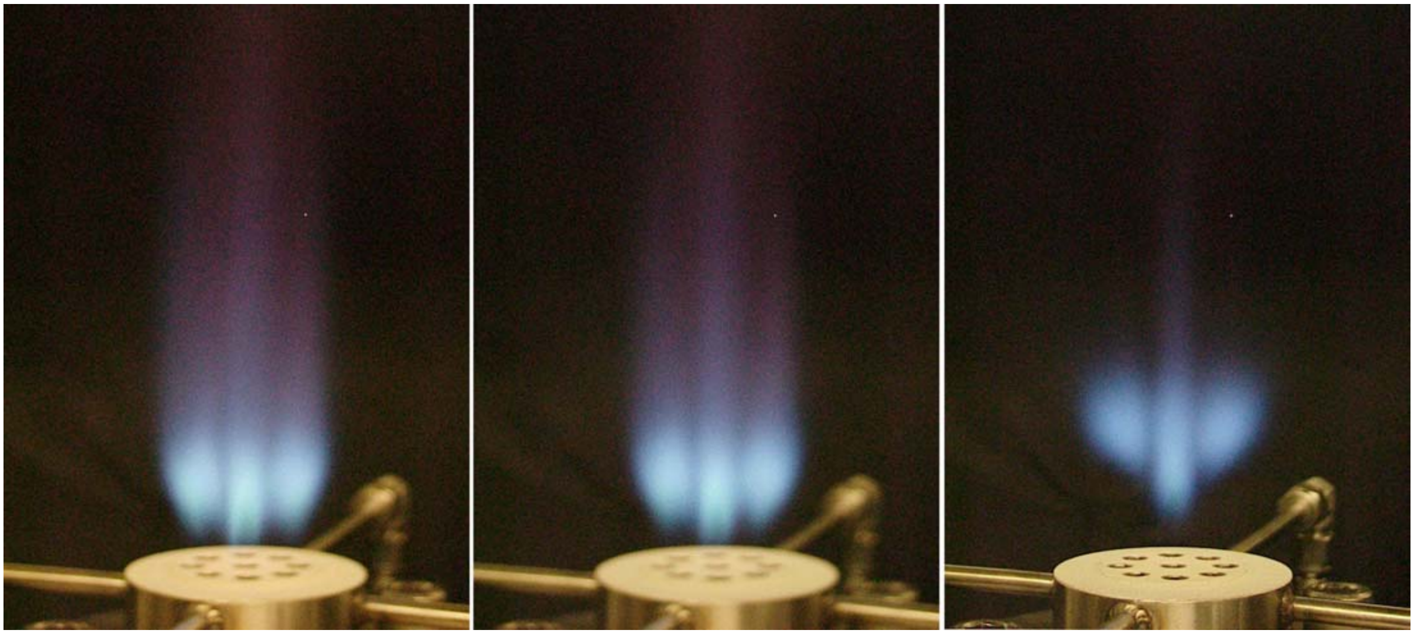

Fig. 4. Direct flame luminosity photographs for unconfined flame. n_{H2}=0.9, u=30 m/s (98.4 ft/s) a) ϕ=0.9; b) ϕ=0.74; c) ϕ=0.68. Photographs taken at F2.2, 1/30 second exposure.

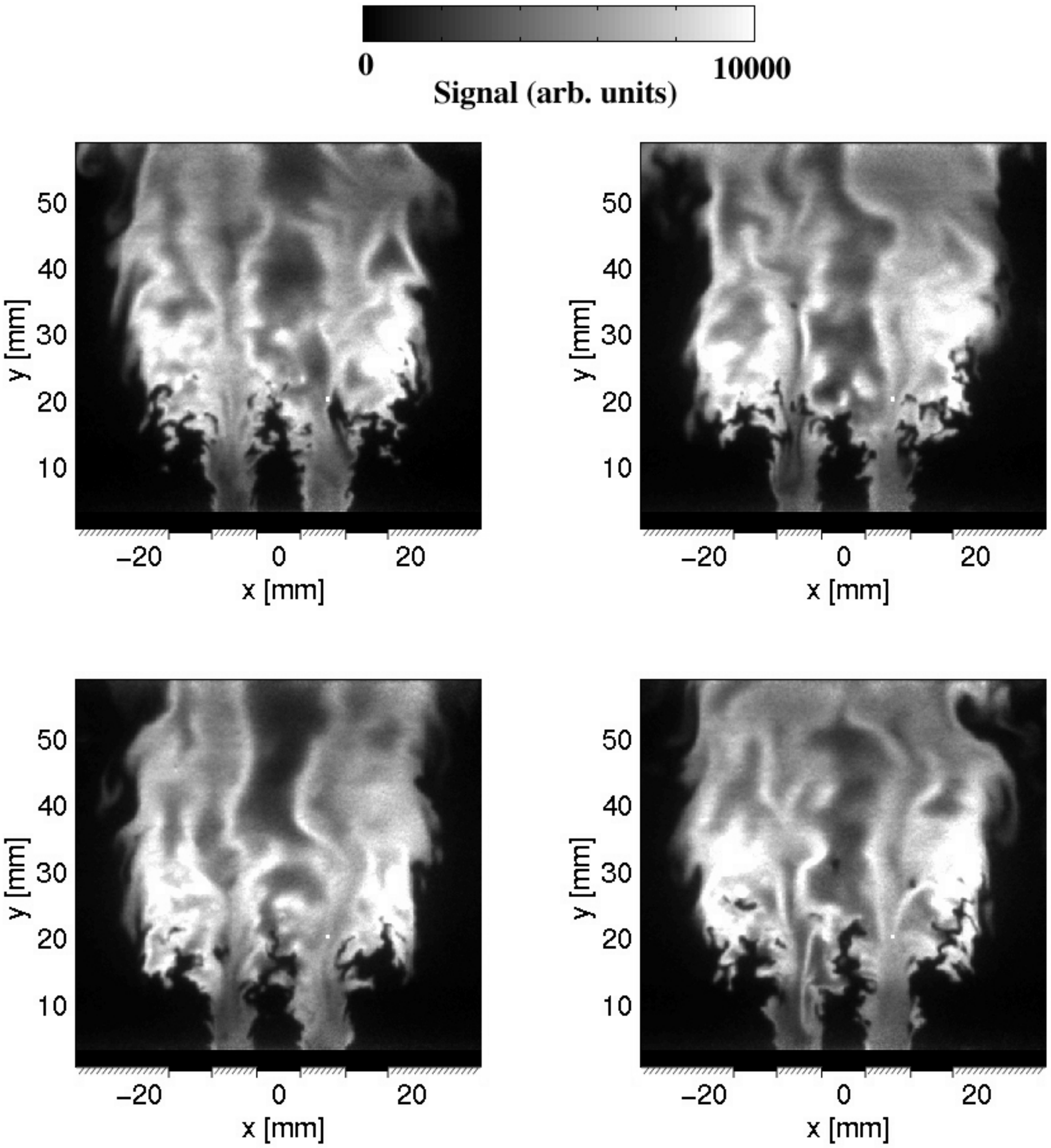

Fig. 5a. OH PLIF images in unconfined flame. n_{H2}=0.9, u=30 m/s (98.4 ft/s), ϕ=0.90. The false color gray scale varies linearly with OH mole fraction. The images correspond to point **a** in Fig. 3.

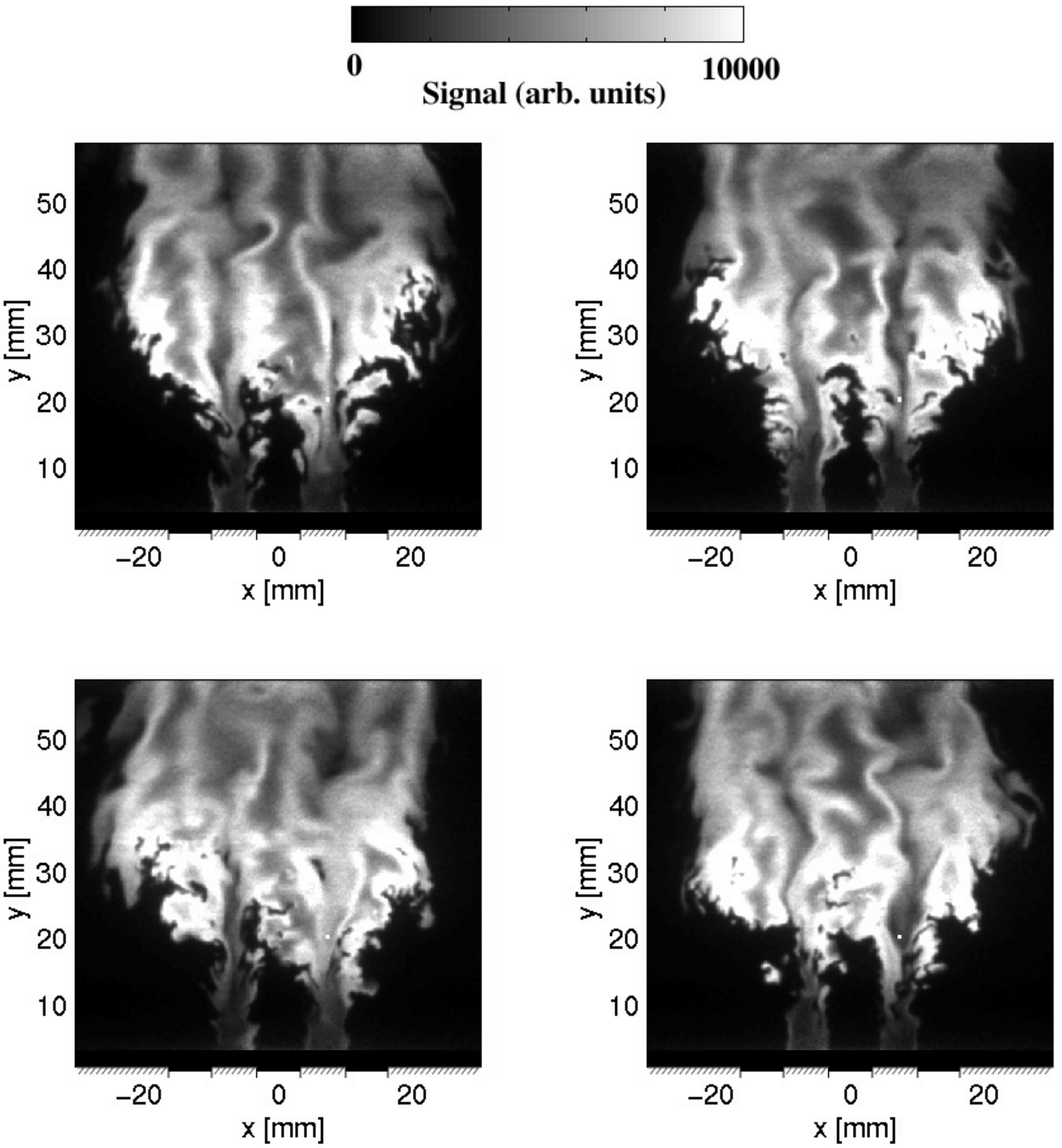

Fig. 5b. OH PLIF images in unconfined flame. n_{H2}=0.9, u=30 m/s, (98.4 ft/s) ϕ=0.74. The images correspond to point **b** in Fig. 3.

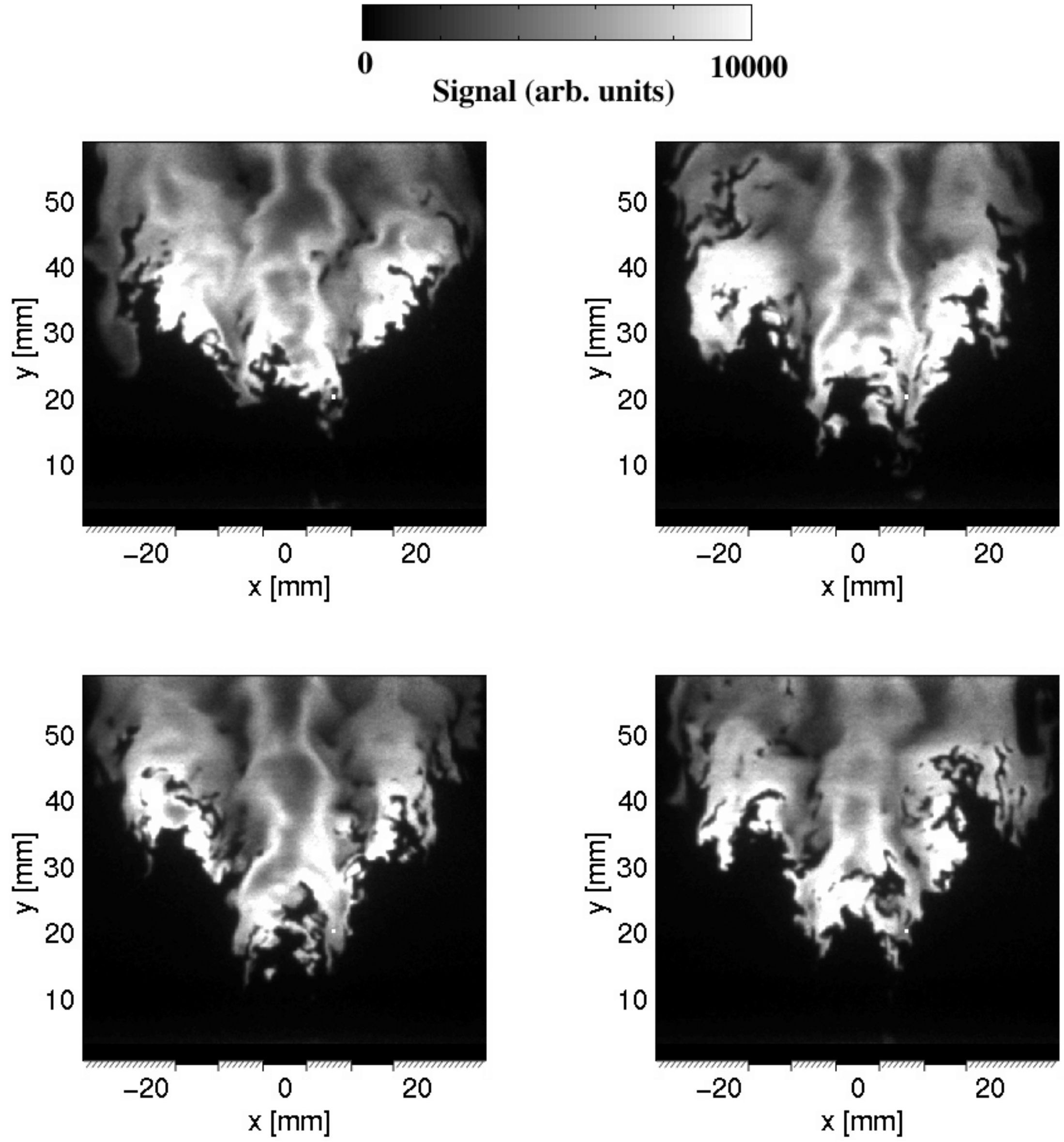

Fig. 5c. OH PLIF images in unconfined flame. n_{H2}=0.9, u=30 m/s (98 ft/s), ϕ=0.68. The images correspond to point **c** in Fig. 3.

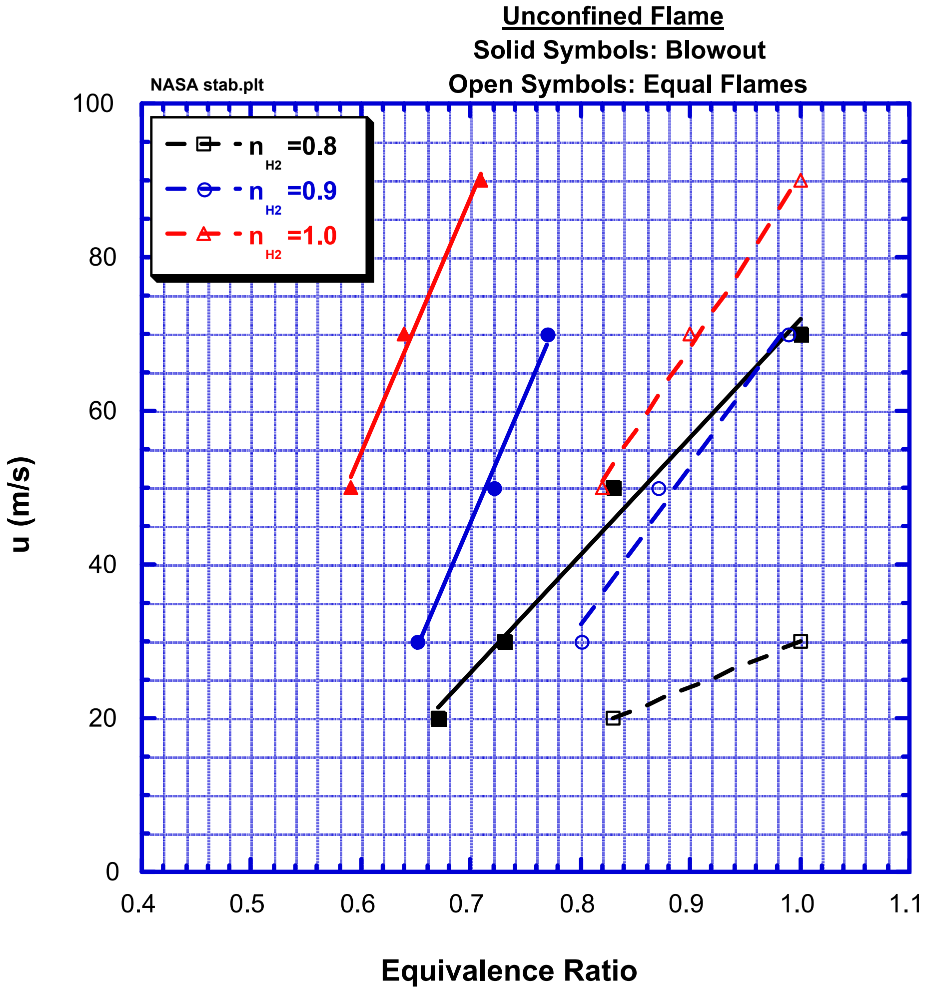

Fig. 6. Effect of hydrogen addition on burner flame regime and stability map. Unconfined flame.

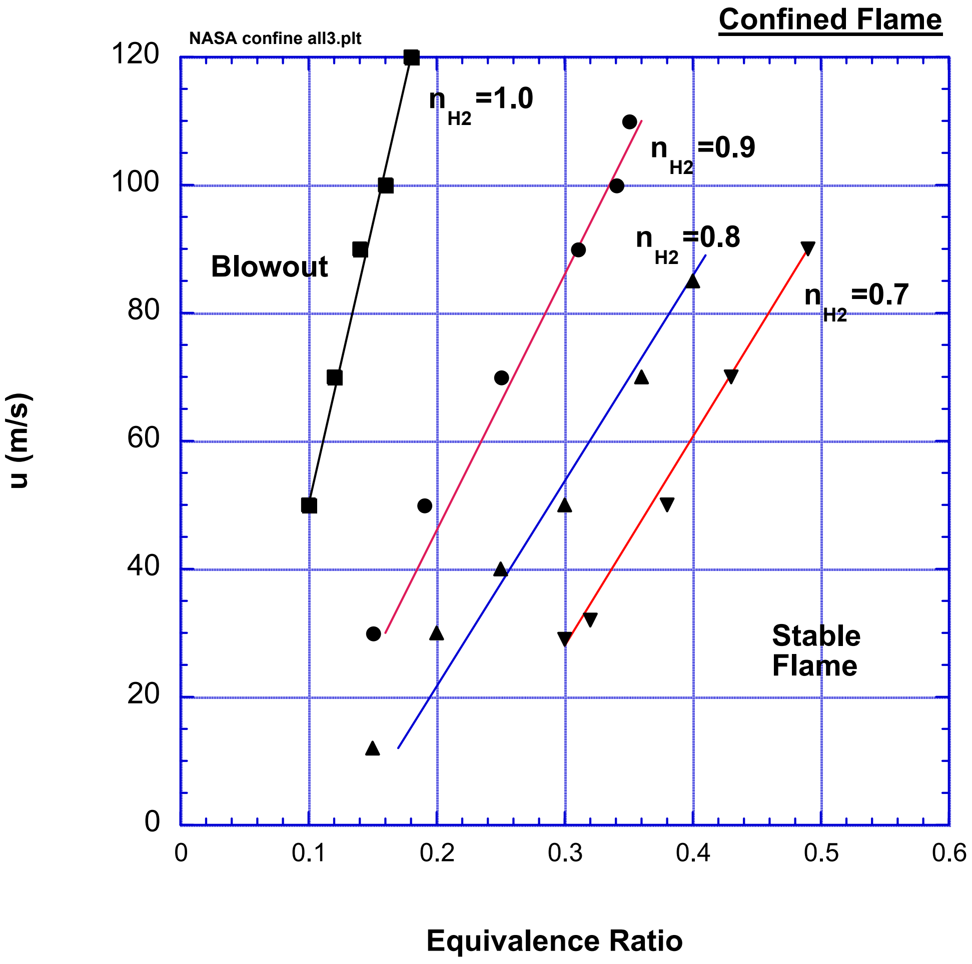

Fig. 7a. Effect of hydrogen addition on burner blowout map. Confined flame.

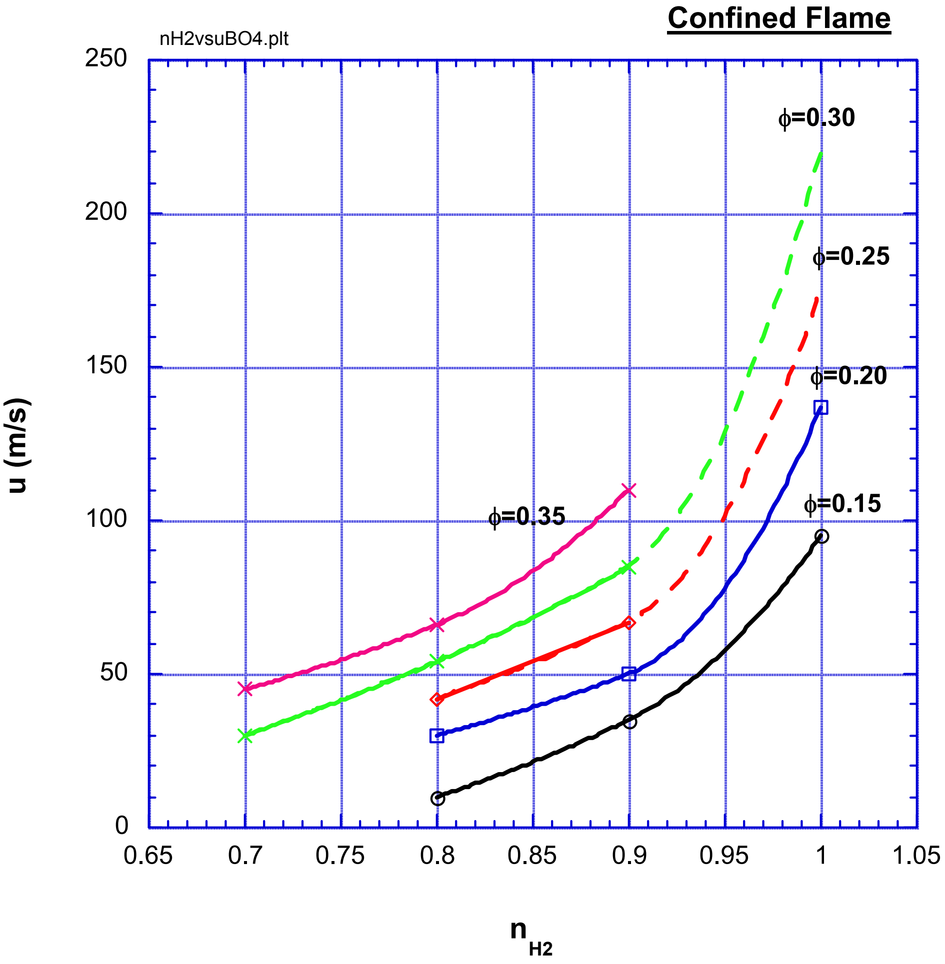

Fig. 7b. Effect of hydrogen addition on burner blowout map. Confined flame.

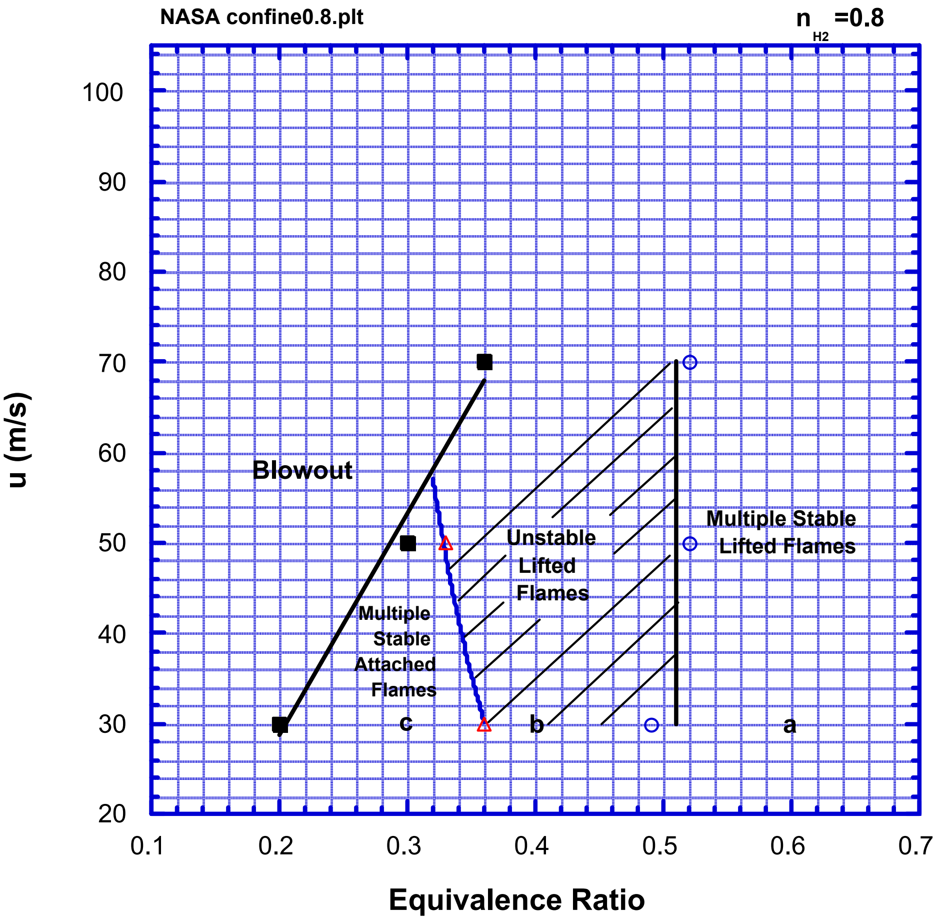

Fig. 8. Detailed flame regime and stability map for n_{H2}=0.8. Confined flame.

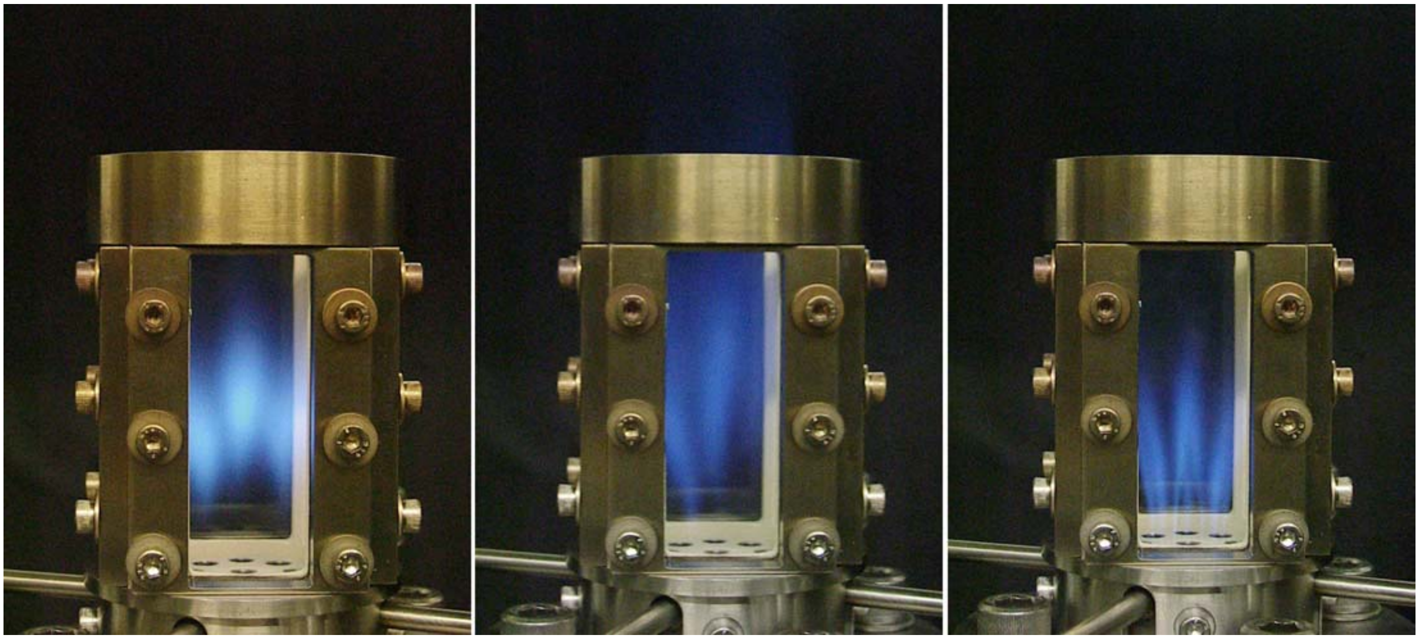

Fig. 9. Direct flame luminosity photographs for confined flame. n_{H2}=0.8, u=30 m/s.(98.4 ft/s) a) ϕ=0.6; b) ϕ=0.4; c) ϕ=0.3. Photographs taken at F2.2, 1/30 second exposure.

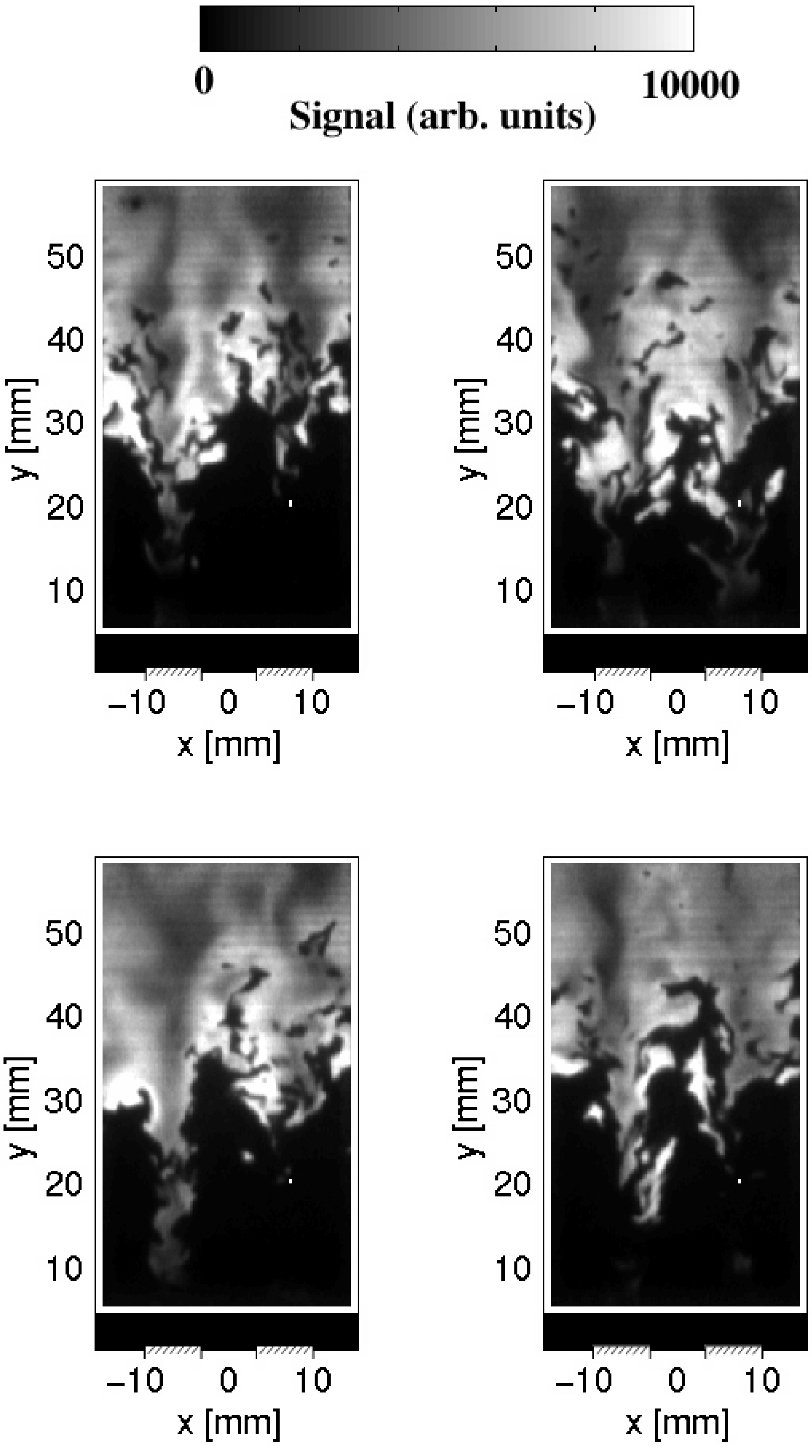

Fig. 10a. OH PLIF images in confined flame. $n_{H2}=0.8$, u=30 m/s (98.4 ft/s), $\phi=0.60$. The images correspond to point **a** in Fig. 8.

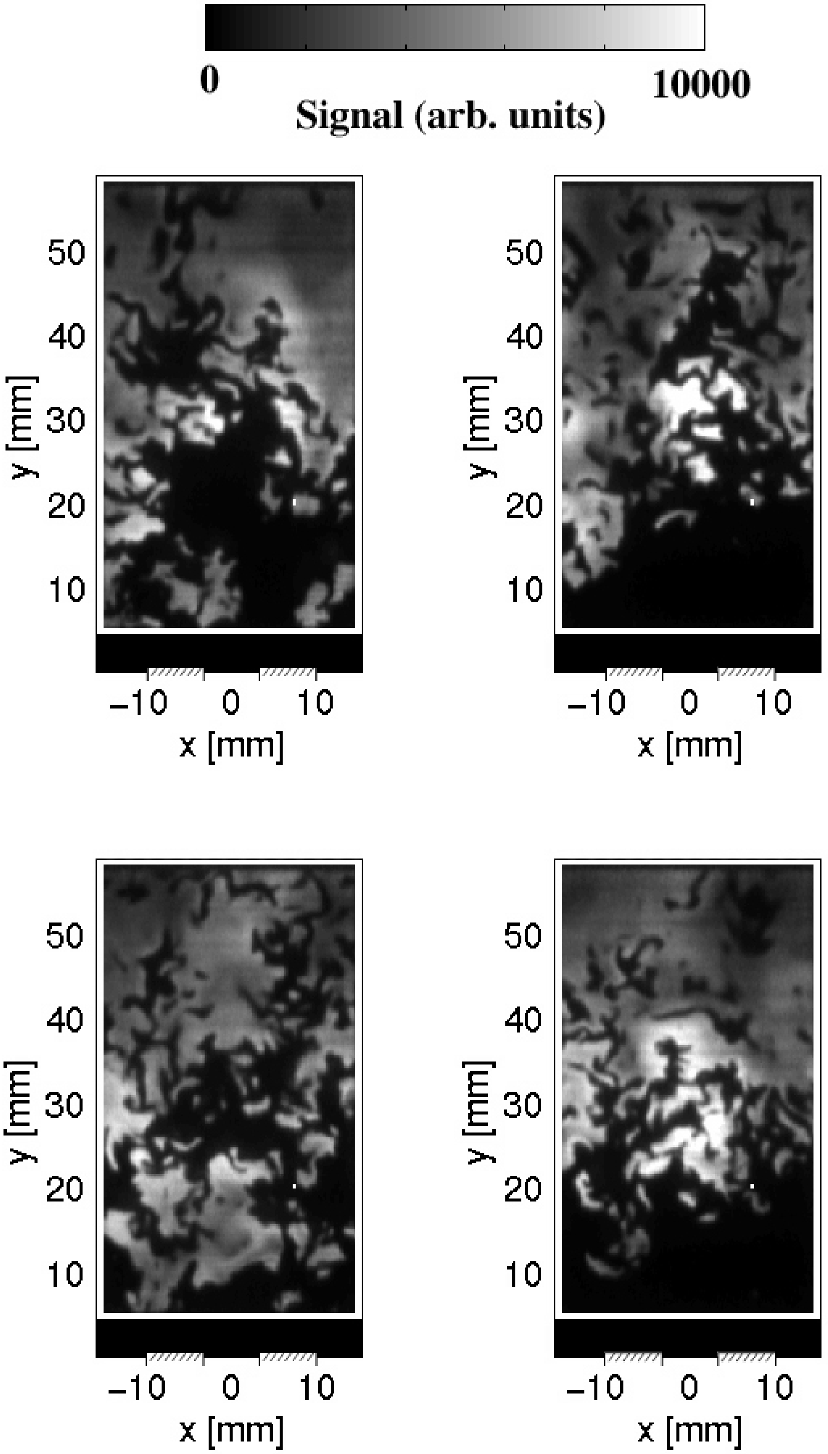

Fig. 10b. OH PLIF images in confined flame. n_{H2}=0.8, u=30 m/s (98.4 ft/s), ϕ=0.40. The images correspond to point **b** in Fig. 8.

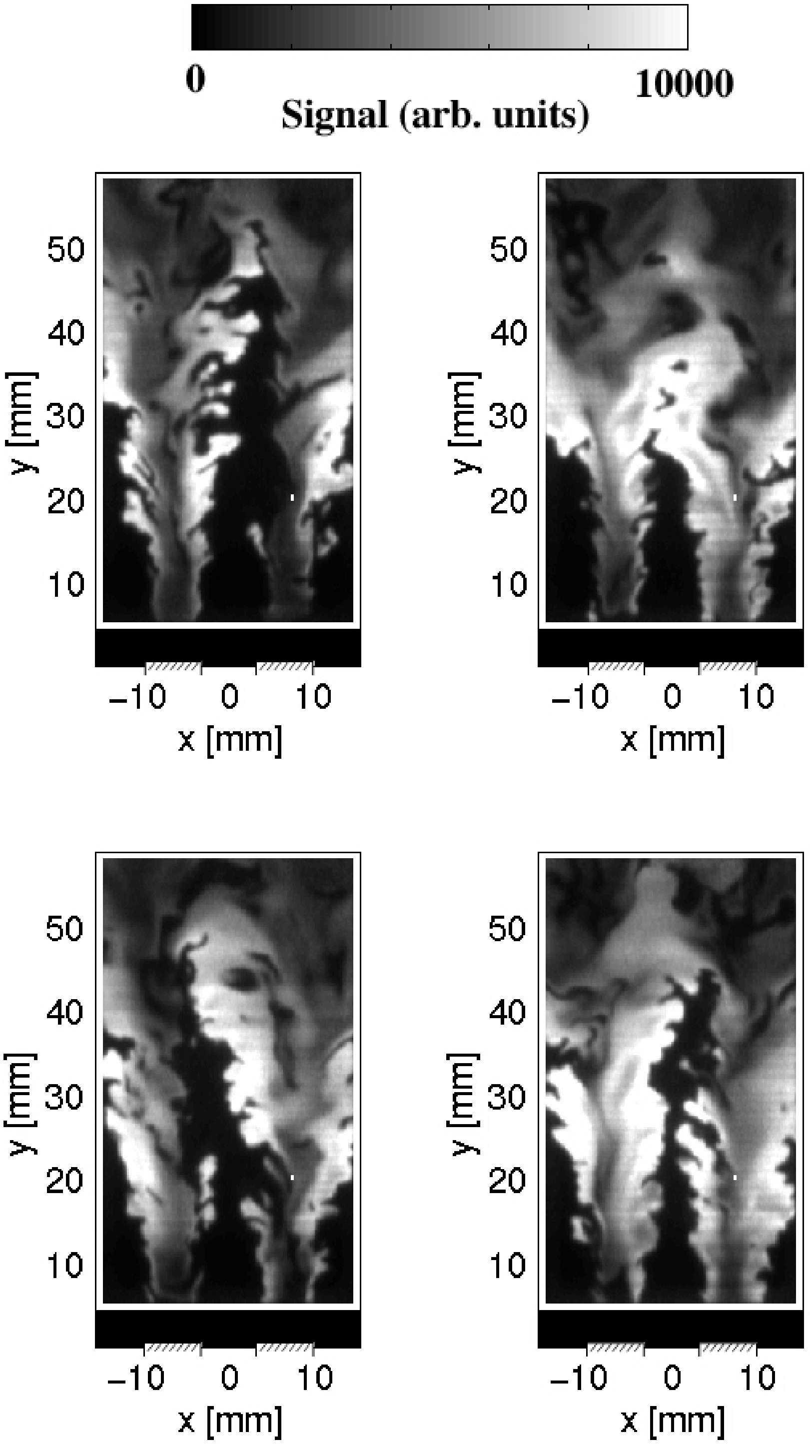

Fig. 10c. OH PLIF images in confined flame. n_{H2}=0.8, u=30 m/s (98.4 ft/s), ϕ=0.30. The images correspond to point **c** in Fig. 8.

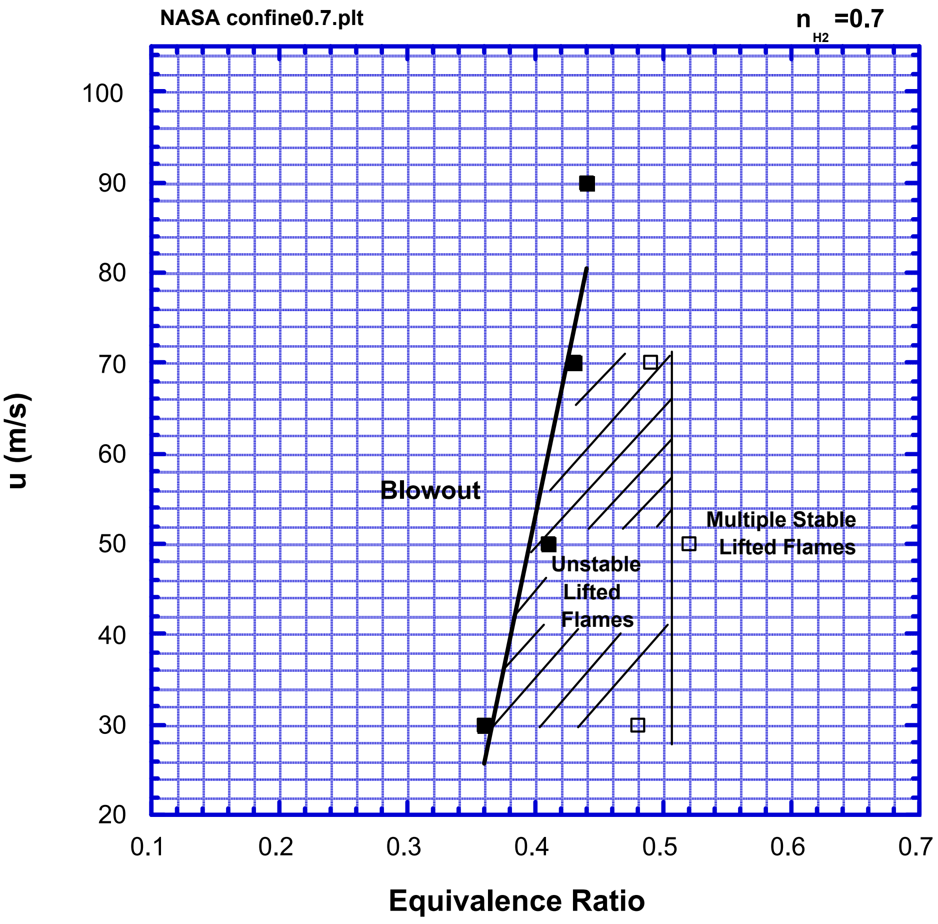

Fig. 11. Detailed flame regime and stability map for n_{H2}=0.7. Confined flame.

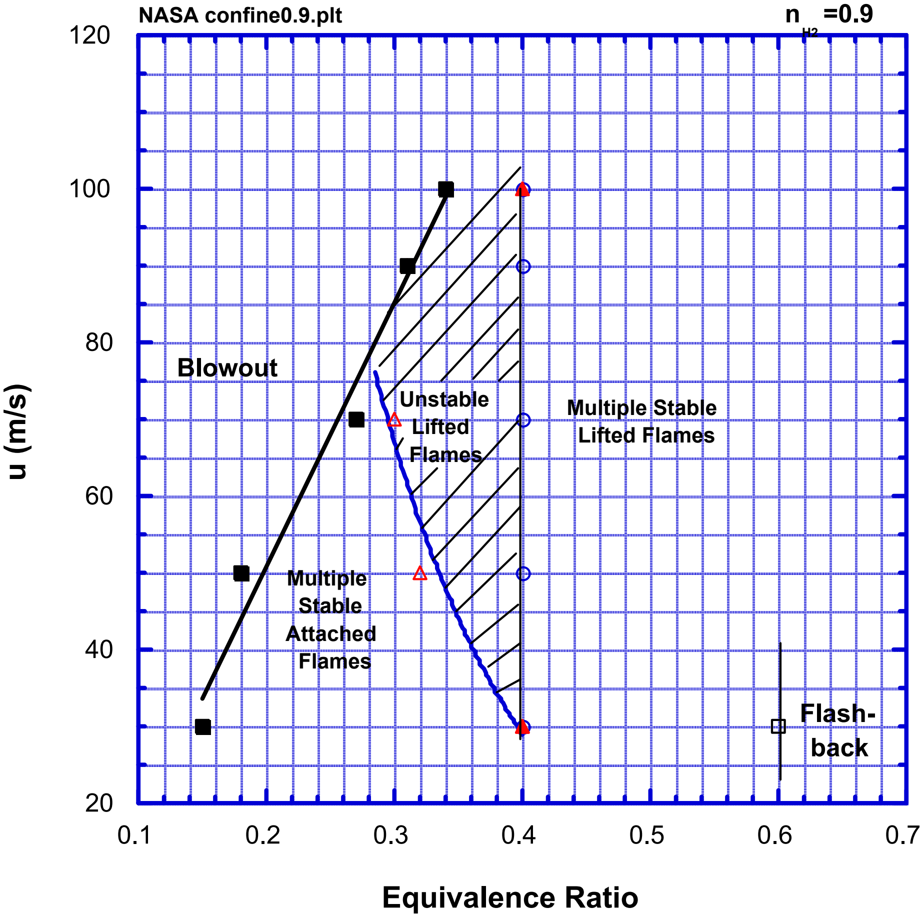

Fig. 12. Detailed flame regime and stability map for n_{H2}=0.9. Confined flame.

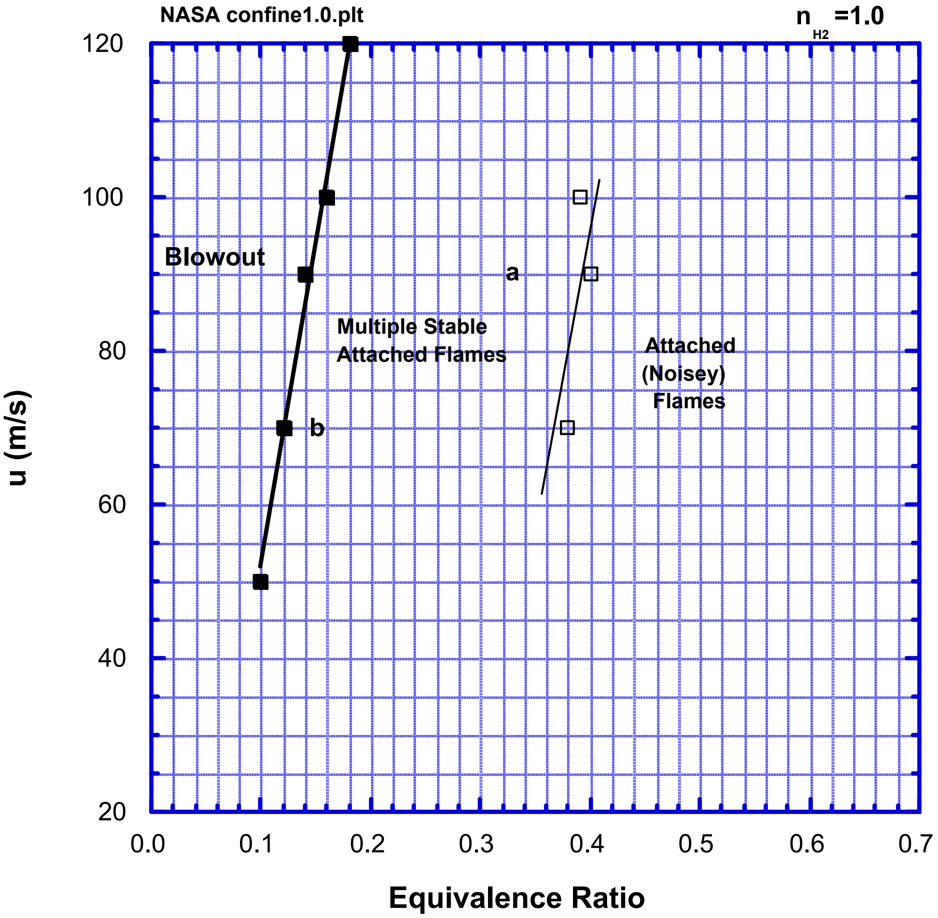

Fig. 13. Detailed flame regime and stability map for n_{H2}=1.0. Confined flame.

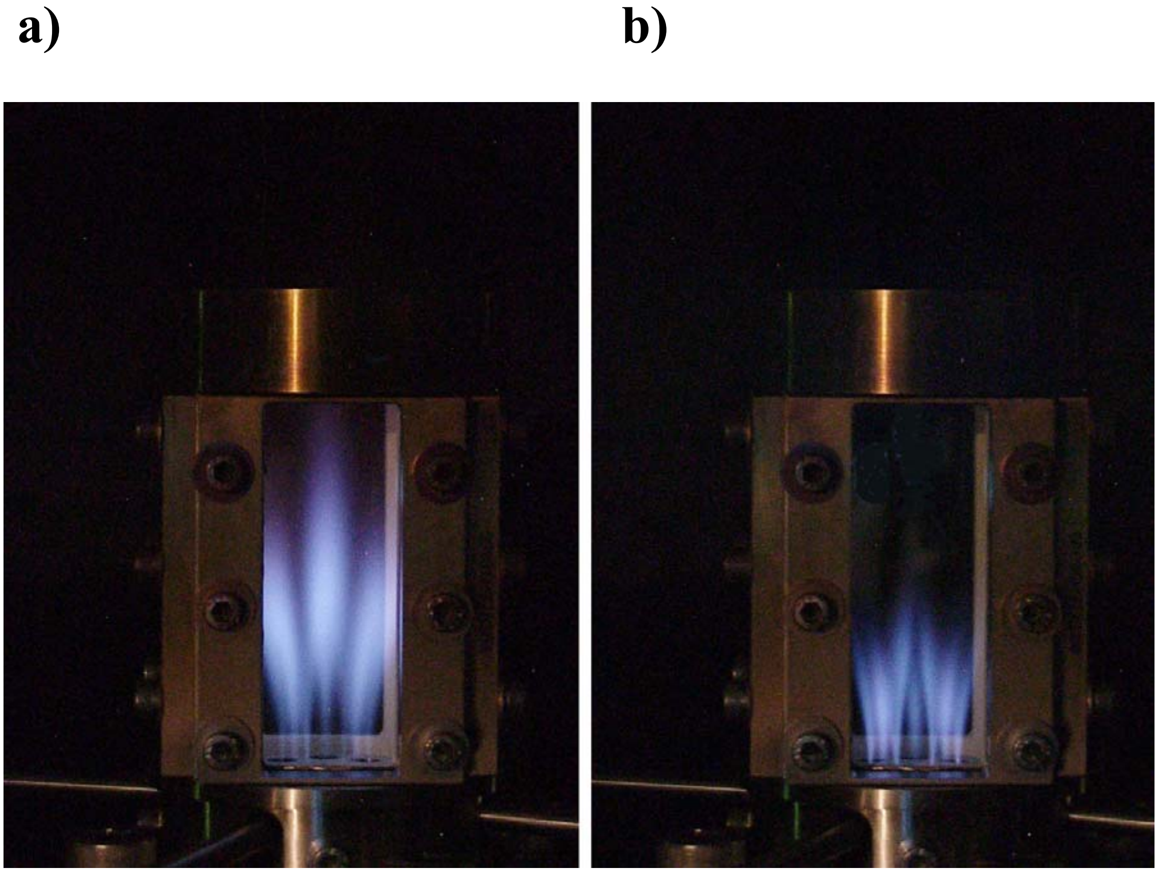

Fig. 14. Direct flame luminosity photographs for confined flame. n_{H2}=1.0. a) u=90 m/s (295 ft/s) , ϕ=0.33; b) u=70 m/s (230 ft/s), ϕ=0.15. Photographs taken at F2.4, 0.6 second exposure.

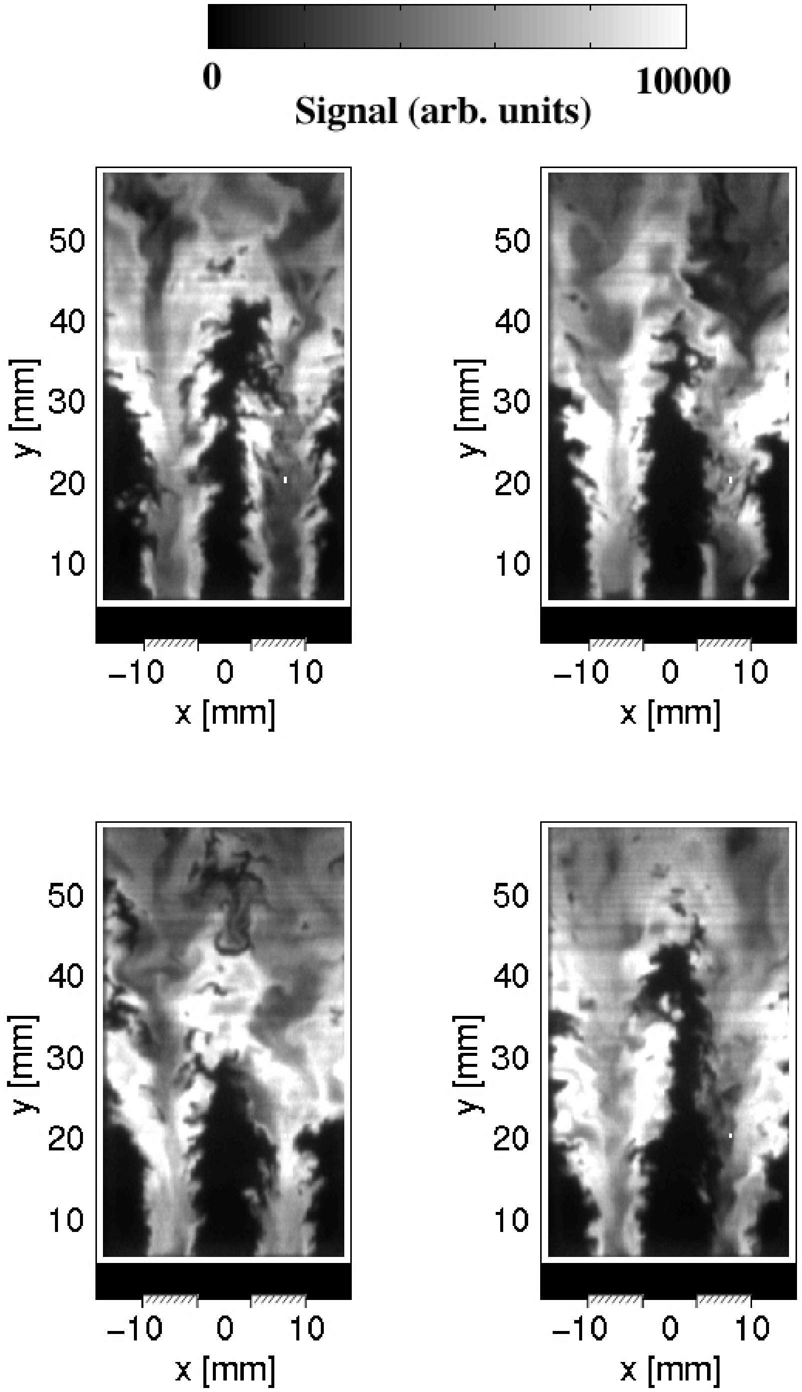

Fig. 15a. OH PLIF images in confined flame. n_{H2}=1.0, u=90 m/s (295 ft/s), ϕ=0.33. The images correspond to point **a** in Fig. 13.

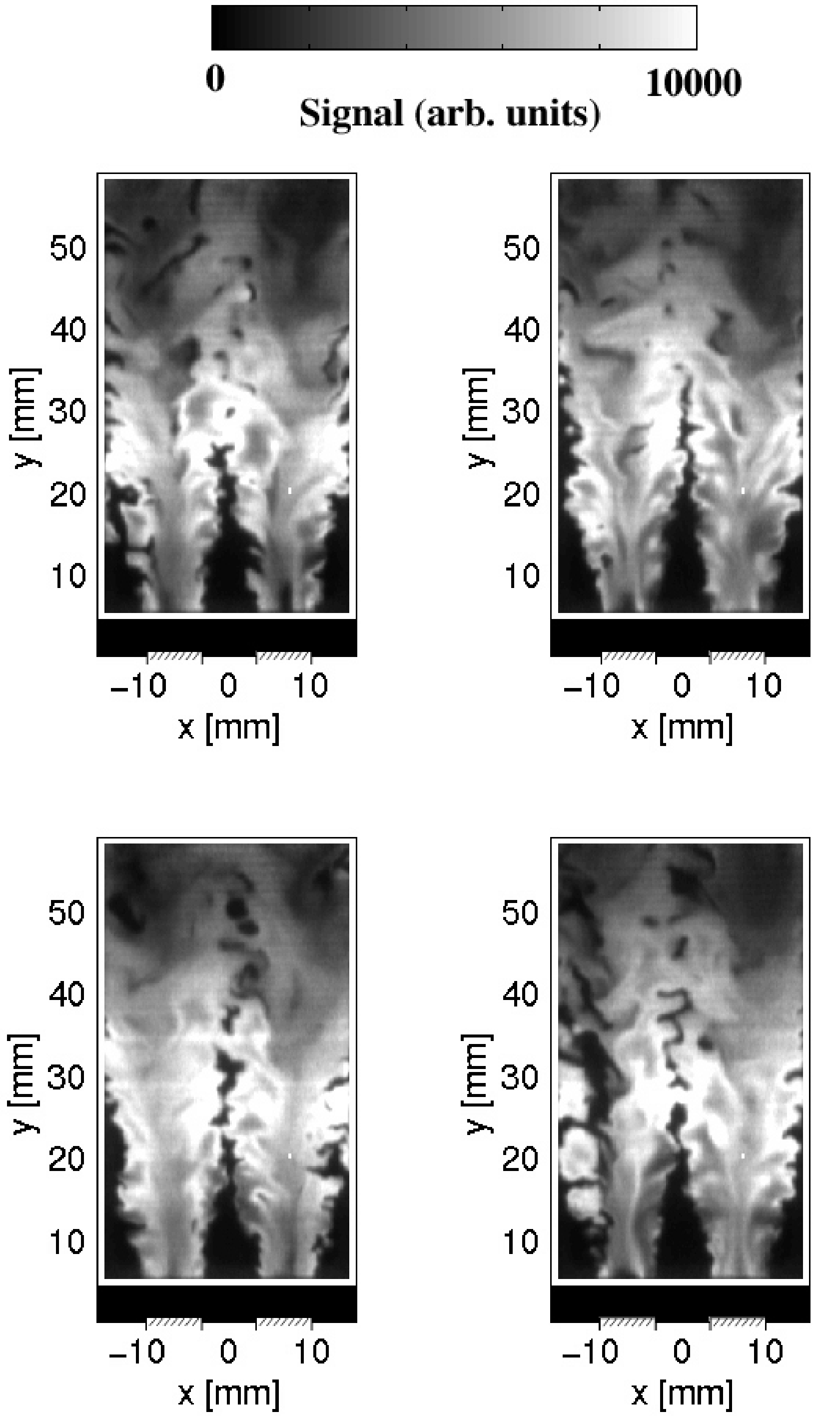

Fig. 15b. OH PLIF images in confined flame. n_{H2}=1.0, u=70 m/s (230 ft/s), ϕ=0.15. The images correspond to point **b** in Fig. 13.

Fig. 16. High resolution photograph of flame in Fig. 12 a). n_{H2}=1.0, u=90 m/s (295 ft/s), ϕ=0.33. Photographs taken at F2.4, 0.6 second exposure.

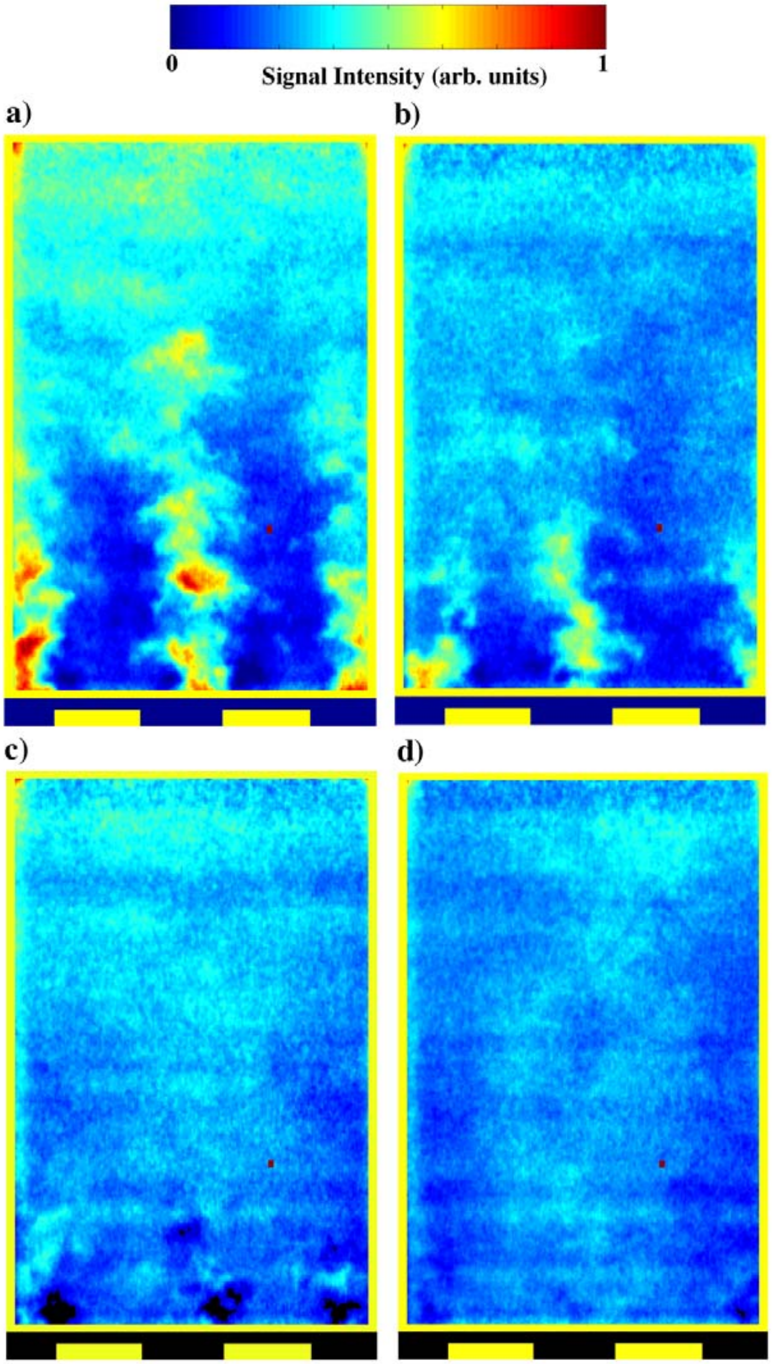

Fig. 17. Acetone PLIF images in confined flow at various fuel-jet to primary-air momentum ratios. a) J =3.82; b) J =5.97; c) J =10.61; d) J =23.9.

Distribution

Printed copies sent through the mail

20 Dr. Timothy Smith
NASA Glenn Research Center
21000 Brookpark Road
MS 5-10, Rm 263
Cleveland OH 44135

1 Geo Richards
S. Department of Energy
National Energy Technology Center
P.O. Box 880, Mail stop: N05
(ST-20, Office:B26-102)
Morgantown, WV 26507-0880

1 Dan Maloney
U.S. Department of Energy
National Energy Technology Center
P.O. Box 880, Mail stop:N05
Morgantown, WV 26507-0880

1 Steven Woodruff
U.S. Department of Energy
National Energy Technology Center
P.O. Box 880, Mailstop: N05
(ST-20, Office:B26-102)
Morgantown, WV 26507-0880

1 Bryan Towns
Chemical Engineer
Energetics, Inc.
901 D Street, Suite 100
Washington D.C. 20024

1 Ajay Agrawal
School of Aerospace and Mechanical Engineering
865 Asp Ave.
Room 217
Norman, OK 73019-0601

1		Don Wicksall School of Aerospace and Mechanical Engineering 865 Asp Ave.Room 212 Norman, OK 73069
1		Gerald A. Hollins Evesto, Inc. 681 Abbot Ave. Daly City, CA 94014
1		Ray Hobbs Senior Consulting Engineer Technology Development Pinnacle West Capital Corporation 400 North 5th Street, MS 2624 Phoenix, AZ 85004
1		Peter Stuttaford Combustion Engineering Manager Power Systems Manufacturing 1440 West Indiantown Rd., Suite 200 Jupiter, FL 33458
1	MS9051	Joe Oelefein
15	MS9051	Robert Schefer
1	MS9054	Don Hardesty
1	MS9053	Jay Keller
1	MS9051	Andy McIlroy
3	MS 9018	Central Technical Files, 8945-1
1	MS 0899	Technical Library, 9616
1	MS 9021	Classification Office, 8511/Technical Library, MS 0899, 9616 DOE/OSTI via URL

Electronic copies (PDF files) sent via email

1 Steve Chalk
Program Manager
EE-2H/Forrestal Building
U.S. Department of Energy
1000 Independence Ave, SW
Washington, DC 20585

1 Neil Rossmeissl
General Engineer
EE-2H/Forrestal Building
U.S. Department of Energy
1000 Independence Ave, SW
Washington, DC 20585

1 Sigmund Gronich
General Engineer
EE-2H/Forrestal Building
U.S. Department of Energy
1000 Independence Ave, SW
Washington, DC 20585

1 Arlene Anderson
Physical Scientist
EE-2H/Forrestal Building
U.S. Department of Energy
1000 Independence Ave, SW
Washington, DC 20585

Harry Morehead
Manager, New Program Development
Siemens Westinghouse Power Corp.
4400 Alafaya Trail, MC 381
Orlando, FL 32836-2399

1 Dr. Jack Solomon
Praxair Inc.
39 Old Ridgebury Road
Danbury, CT 06810-5113

1 Tom Dalton
Praxair Inc.
39 Old Ridgebury Road
Danbury, CT 06810-5113

This page intentionally left blank